SEDIMENTOLOGY AND STRATIGRAPHY OF HIGH-LATITUDE, GLACIGENIC DEPOSITS FROM THE LATE PALEOZOIC ICE AGE IN THE TEPUEL-GENOA BASIN, PATAGONIA, ARGENTINA

by

Sarah R. Survis

A Thesis Submitted in

Partial Fulfillment of the

Requirements for the Degree of

Master of Science

in Geosciences

at

The University of Wisconsin-Milwaukee

August 2015

ABSTRACT

SEDIMENTOLOGY AND STRATIGRAPHY OF HIGH-LATITUDE, GLACIGENIC DEPOSITS FROM THE LATE PALEOZOIC ICE AGE IN THE TEPUEL-GENOA BASIN, PATAGONIA, ARGENTINA

by

Sarah R. Survis

The University of Wisconsin-Milwaukee, 2015
Under the supervision of Dr. John Isbell

The Late Paleozoic Ice Age (LPIA) was the longest lived ice age of the Phanerozoic lasting ~87 million years. During this time multiple, small ice sheets advanced and retreated with alternating glacial and nonglacial intervals across Gondwana. Controversy still remains over the size, timing, and number of ice sheets because the traditional view of Gondwana during this time is of a single, large ice sheet that waxed and waned across the supercontinent. Furthermore, high-latitude glacially-influenced basins during the Carboniferous have received limited attention, underscoring the poor understanding of glacial to non-glacial transitions. The Tepuel Basin in Patagonia, Argentina, was located within the south polar circle through much of the LPIA, and contains a near complete sedimentary record of the Carboniferous through the Early Permian due to high subsidence rates in an outer shelf, basin slope, and basin floor setting. The strata within the Pampa de Tepuel contain sandstones, some reworked by waves, mudstone containing fossils and lonestones, conglomerates, and diamictites. Six stratigraphic sections were examined along an outer shelf to basin slope environment and the strata are divided into eight lithofacies associations which are: 1) massive mudrock 2) thin-bedded sandstone and mudstone, 3) deformed and undeformed sediment blocks,

4) thick-bedded wave-rippled sandstone, 5) large-scale loaded sandstone 6) conglomerate and massive sands, 7) two diamictite subfacies, and 8) thrust-faulted, massive, boulder-bearing sandstone. Evidence was found for a glacial advance to the shelf edge, and evidence for seismic activity was seen in large loaded sandstone deposits within the wave-rippled sandstone facies, which are interpreted to be seismites. The sequence stratigraphy of the area suggests that a forced regression occurred, allowing for coarser clastics to be deposited further out in the basin, followed by a rapid transgression. The strata within the study area contain fossils of the *Lanipustula* Biozone, which is considered to range from Serpukovian to early Moscovian in age. Glaciation was occurring in polar Gondwana at this time, and the glaciation was associated with a drop in sea level. This research aids our understanding of the stratigraphy of high-latitude, glaciomarine shelf systems and in understanding of the late Paleozoic Ice Age.

To

my nephew, Domanic

and

my niece, Adeline

TABLE OF CONTENTS

LIST OF FIGURES

LIST OF TABLES

ACKNOWLEDGEMENTS

First and foremost, I want to thank my advisor, Dr. John Isbell, for all of his guidance and support. This project would not have been possible without his help. I cannot express enough how much I appreciate all of the guidance I've received from him, both as a graduate student and an undergraduate. I would not be the scientist I am today without him. I would also like to thank Dr. Bill Kean and Dr. Erik Gulbranson for being a part of my committee and providing me with helpful suggestions and insights for my thesis. Thank you to Dr. Paul Price, as well, from UW-Washington County for initially sparking my interest in geology and convincing me it would be a good subject pursue.

I would like to express gratitude to our Argentine collogues, Dr. Alejandra Pagani and Dr. Arturo Taboada for their help with biostratigraphy and for answering questions along the way. I also want to thank Kate Pauls for her assistance in the field, for her help in the office, and for laughing with me through the stressful times of grad school. And thank you to Santiago Bessone, Nicole Braun, and Neil Griffis for your help in the field and for the great memories from Argentina.

Thank you to the Center for Latin American and Caribbean Studies, Wisconsin Geologic Society, and the UWM Geosciences Department for their financial support of this project in Patagonia, and thank you to the Museo Paleontológico Egidio Feruglio (MEF) for allowing us to accompany your scientists into the field.

I want to express my gratitude to everyone in the Geosciences department at UW-M for all the educational support I've received through the years and thank you to my

fellow grad students for making the past two years fun and memorable. It has been a great pleasure to be a part of this department, and everyone helped to make my time in the department wonderful.

Finally, I would like to sincerely thank my husband, Jacob, my parents, Bruce and Judy, and my siblings and their spouses, Paul, Maria, Jill and Brian, for their continuous support throughout this process. And thank you Adel, Gloria, and Sara for supporting me as well. I appreciate all of the love and assurance I've received from all of you, and I would not be where I am without your support.

1. Introduction

The Late Paleozoic Ice Age (LPIA; 346-259 million years ago) was the longest-lived ice age of the Phanerozoic. The glacial interval was an important climatic event because it represents the only complete record of the transition from an icehouse to a greenhouse state for a biologically complex Earth (Montanez and Poulsen, 2013). The traditional view of the LPIA, which persists to this day, is that of a single large ice sheet that waxed and waned continuously across Gondwana for up to 100 million years (Ziegler et. al., 1997; Blakey, 2008; Buggisch et. al., 2011). However, more recent work in Australia, Antarctica, South Africa, and southern South America identify the occurrence of multiple, smaller ice sheets that advanced and retreated diachronously across the supercontinent with alternating glacial and nonglacial/interglacial intervals ranging from 1-8 million years (Figure 1) (Lopez-Gamundi, 1997; Visser, 1997; Isbell et. al., 2003, 2008a, 2008b, 2012; Fielding et al., 2008a, 2008b, 2008c; Henry et al., 2008, 2010, 2012; Mory et al., 2008; Birgenheier et al., 2009; Gulbranson et al., 2010; Montanez and Poulsen, 2013). Despite recent advances, the number of ice sheets, the size of the ice sheets, and the timing of glacial events remain controversial. Many of the records from the various Gondwana crustal blocks are composite records stitched together from widely spaced outcrops. Because of this, the recent work results in an improved, but incomplete view of the glaciation. The current polar record is derived mainly from Antarctica, which was situated over the South Pole throughout most of the late Paleozoic. However, that record is incomplete as an unconformity separates Devonian strata below from Permian glacial deposits above (Isbell et al., 2008a, 2010). Therefore, there is a need for continued refinement of the record.

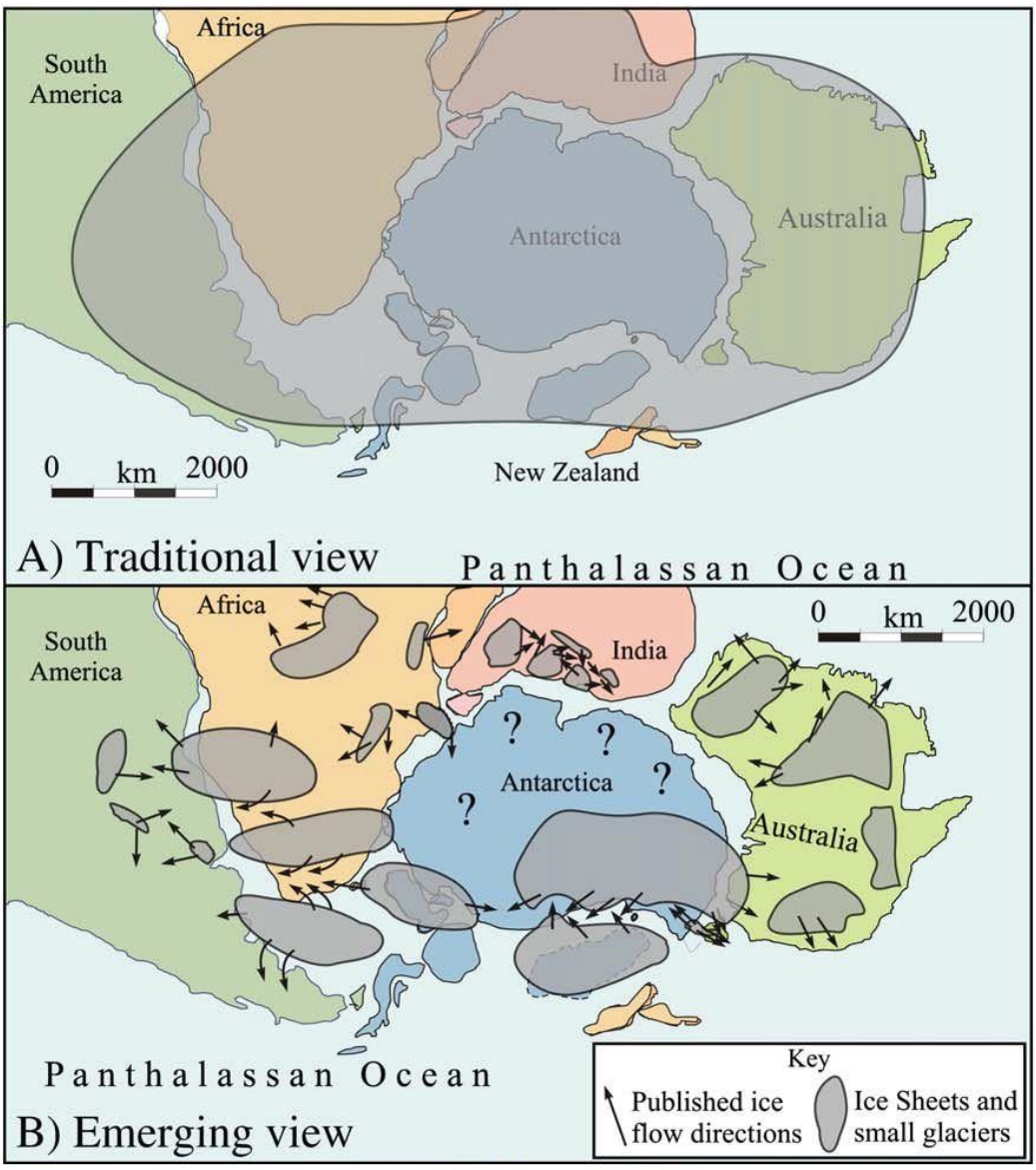

Figure 1. Traditional and emerging views of glaciation during the late Paleozoic Ice Age. A) The traditional view is of a single, large ice sheet. B) The emerging view is of multiple, smaller ice sheets and small glaciers at their maximum extent during the Gzhelian to early Sakmarian (Pennsylvanian–Early Permian). From Isbell et al., 2010.

The LPIA is believed to have begun during the Visean in Western South America(cf. Gulbranson et al., 2010). However, both Late Devonian and Early Mississippian glacigenic deposits have also been reported from South America (cf. Caputo et al., 2008). The maximum extent in Gondwana occurred during the Late Pennsylvanian to Early Permian (Isbell et al., 2012), and ending during the Capitanian to Wuchiapingian in eastern Australia (Fielding et al., 2008c; Isbell et al., 2012; Frank et al., 2015). Throughout much of this glaciation, the South Pole was located in Antarctica with southern South America (Patagonia), southern-most Africa, and Tasmania located within the polar circle (Figure 2). The polar record from the LPIA has been analyzed in detail in Antarctica and to a lesser extent, South Africa and Tasmania (Lindsay, 1970; Isbell et al., 2001, 2008a, 2008b, 2012; Isbell, 2010; Henry et al., 2012; Visser, 1997). However, South Africa and Tasmania were not located within the Polar Circle for the duration of the LPIA. Of these crustal blocks, only Patagonia contains a Mississippian-Permian record of Polar Gondwana.

Gonzalez-Bonorino and Eyles (1995) argue that the LPIA record is mostly a record of ice retreat and that the glacial terrestrial record is discontinuous and poorly preserved. However, due to deposition in a marine high accommodation setting beyond the maximum limit of ice advance, the study of glaciomarine deposits provides an opportunity to establish a near continuous record for the LPIA.

Eustatic changes in sea level for the late Paleozoic, as derived from the far-field (low-latitude) record, are well established (cf. Heckel, 1994; Eros et al., 2012). However, the near field record of ice volume changes and their effect on world sea level is less well

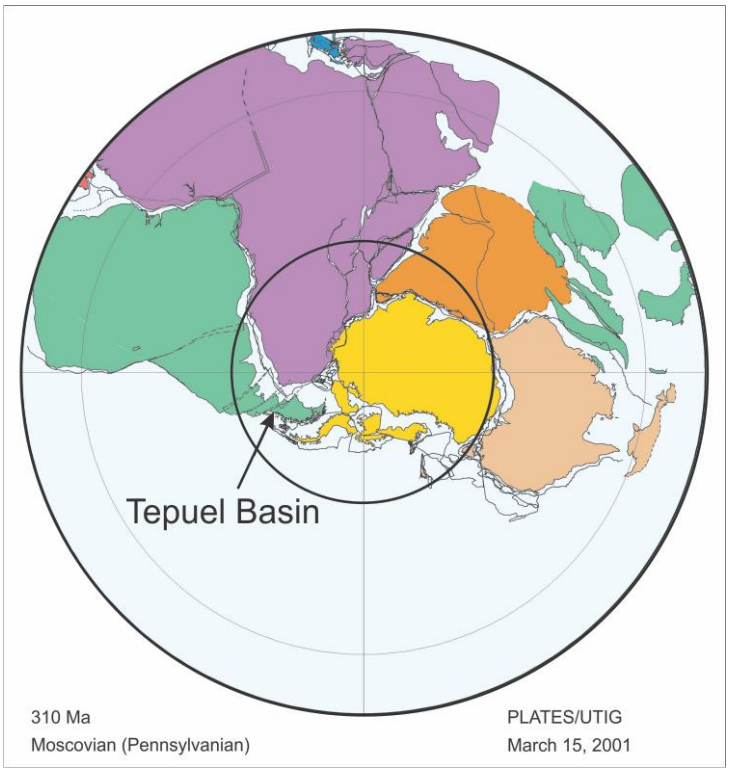

Figure 2. Plate reconstruction of Gondwana during the Late Paleozoic at 310 Ma. The reconstruction is from the Plates Project, UTIG, 2001; Pauls, 2014.

constrained (Isbell et al., 2003). In terms of sequence stratigraphy, on low latitude, non-glaciated shelves, facies changes occur due to changes in relative sea level and sediment supply. Whereas, high latitude glaciated shelves respond to changes in eustacy, glacial advance and retreat, sediment supply, and glacial isostatic loading (Boulton, 1990; Powell and Cooper, 2002). The shelf proximal to a high latitude polar (cold based) glacier may not have thick interglacial wedges like temperate glaciated shelves, and the upper slope will be dominated by debris flow diamictites compared to sorted sediment on a temperate glacial upper slope (Powell and Cooper, 2002). Therefore, records from high latitude locations are needed to better understand the climate record during the LPIA and the sequence stratigraphic record associated with glaciated localities.

The Tepuel Basin, located in Chubut Province of Patagonia, Argentina (Figure 3), is an ideal location for studying the LPIA. This area was located within the South Polar Circle throughout much of the Carboniferous and Permian, and it contains a 5,000+ meter thick glacigenic succession of Mississippian to Middle Permian strata (Taboada, 2010). Although these strata were originally hypothesized to have been deposited in subglacial to shallow marine settings (González Bonorino et al., 1988; González Bonorino, 1992; González et al., 1995; González and Diaz Saravia, 2010), a deep water basin is more likely due to the presence of debris flows, turbidites, and other mass transport deposits (cf. Lopez Gamundi et al., 1994; Isbell et al., 2013a). Isbell et al. (2013a) hypothesized

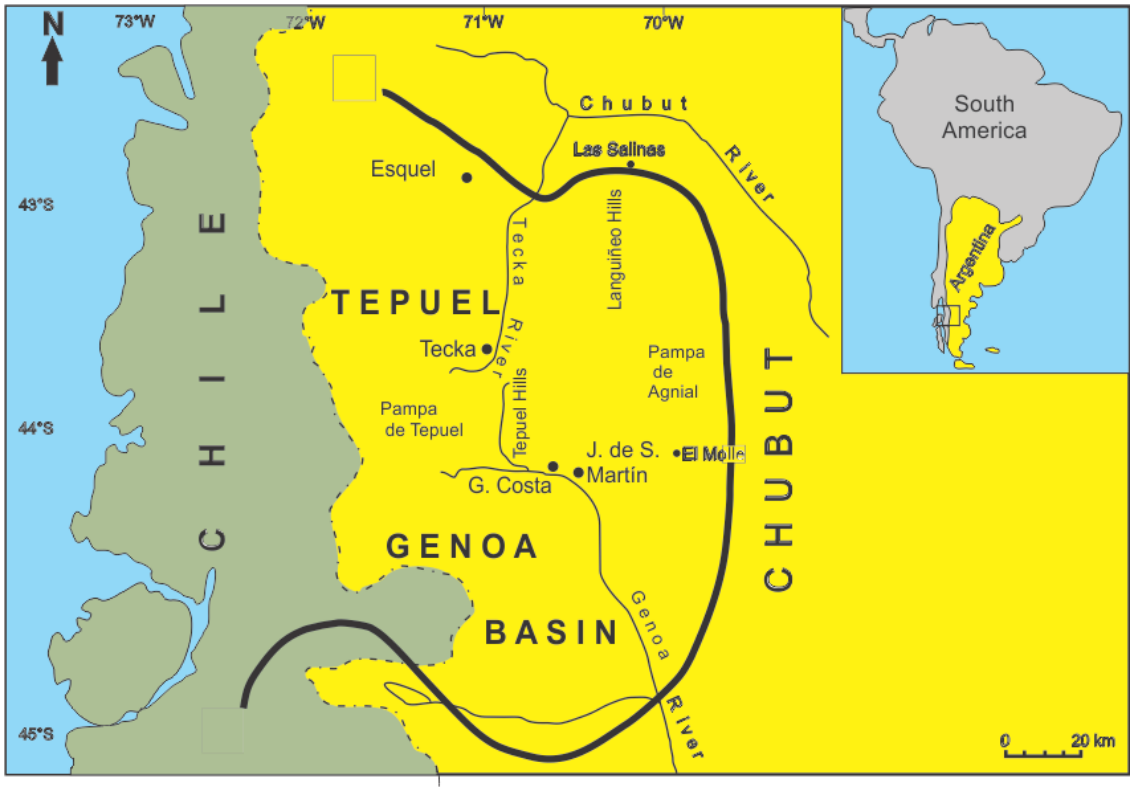

Figure 3. Map of the Tepuel-Genoa Basin located in central Patagonia, Argentina. Modified from Gonzalez and Diaz Saravia, 2010 and Pauls, 2014.

that these strata were deposited in a glacially influenced outer shelf, basin slope and basin floor setting with a relatively high subsidence rate. If this assumption is correct, the succession would provide a near complete polar record of the LPIA (cf. Eyles et al., 1995; Limarino and Spalletti, 2006).

Although an analysis of the entire 5000+ m-thick succession in the Tepuel Basin is underway, it is beyond the scope of this thesis. Here I analyze in great detail a thin interval of this succession to better constrain the environments, the basinal setting, and the nature of glaciation within the depositional basin. A single outcrop within this thick succession was used for this study. Age control is not well established for this basin as no volcanic ash has yet been identified and fossils of the marine invertebrate fauna are partially endemic to this basin. The studied strata is located in the *Lanipustula* Biozone, which is considered to range from Serpukovian to early Moscovian in age (Taboada 2008; 2010; Pagani and Taboada, 2010; Taboada and Shi, 2011; Pauls, 2014). Glacial intervals have been recognized with good age constraints during this interval from other basins in Gondwana (Fielding et al., 2008a, 2008b, 2008c; Gulbranson et al., 2010; Isbell et al., 2012), and glacioeustatic sea level changes have also been hypothesized for this interval (Rygel et al., 2008; Eros et al., 2012). A detailed analysis of the outcrop can give insight into high-latitude sequence stratigraphy in glaciogenic, shelf-edge successions and determine the role glaciation played in the deposition of sediments in this portion of the polar basin. This will also lead to a better understanding of the Tepuel Basin.

1.1 Objectives

The goal of this research project is to understand the depositional processes of proximal glaciers in high-latitude settings. The hypothesis to be tested is that the area contains glacigenic sediment, and it was deposited in a shelf-edge and slope setting during the LPIA (cf. Lopez Gamundi et al., 1994; Isbell et al., 2013a). This study will develop an understanding of glaciomarine settings and add to the polar record for the LPIA, which will aid in understanding global climate change and the nature of glaciations during the late Paleozoic. The objectives are to:

- Evaluate the sedimentary rocks in the area in order to improve the understanding of high-latitude, glacigenic deposits
- Test the hypothesis that deposition occurred in a shelf-edge and slope setting.
- Study deposits from a glaciomarine setting, so a better understanding of LPIA high-latitude, glacially-influenced, sequence stratigraphy can be better understood.
- Contribute to the knowledge of the LPIA in order to help produce a more complete polar record of glaciations in this area.

2. **Geologic Setting**

The Tepuel Basin has a complex tectonic history that is unresolved. It is part of the Patagonian crustal block that is either an allocthonous block or previously attached to southern South America (Rapela et al., 1989; Ramos, 2008; Rapalini et al., 2010; Ramos and Naipauer, 2014). The basin has been interpreted as both a retroarc foreland basin (Eyles et al., 1995; Limarino and Spalletti, 2006) and a forearc basin (Lopez Gamundi, 1997; Ramos, 2008). The retroarc basin interpretation comes from its lack of a volcanic signature within the sediments, its relatively small amount of deformation, and its weak metamorphism (Limarino and Spalletti, 2006). The basin has also been interpreted as a forearc basin due to its characteristics of weak metamorphism and paleocurrents that trend from east to west and its location outboard of a possible volcanic arc (Ramos, 2008). Mesozoic extension followed by Cenozoic compression created the block faulted landscape that is present today in much of the basin (Eyles et al., 1995).

Individual outcrops in the Sierra de Tepuel expose strata of Mississippian to Middle Permian age. Unlike other areas in Gondwana, which have a glacial record that are constructed from widely spaced composite sections, individual 5,000+ meters thick exposures in the Tepuel Basin contain a near complete record of the LPIA (Figure 4) (Limarino and Spalletti, 2006). The strata within the basin are comprised of large bodies of sandstone reworked by waves; thick bioturbated, fossil-bearing mudstone; conglomerates; and diamictites (Andreis et al., 1987; González Bonorino, 1992; Eyles et al., 1995). Within the Tepuel Hills is the Tepuel Group which stratigraphically consists of the Jaramillo, Pampa de Tepuel, and Mojon de Hierro formations (Figure 5) (Taboada and Pagani, 2010).

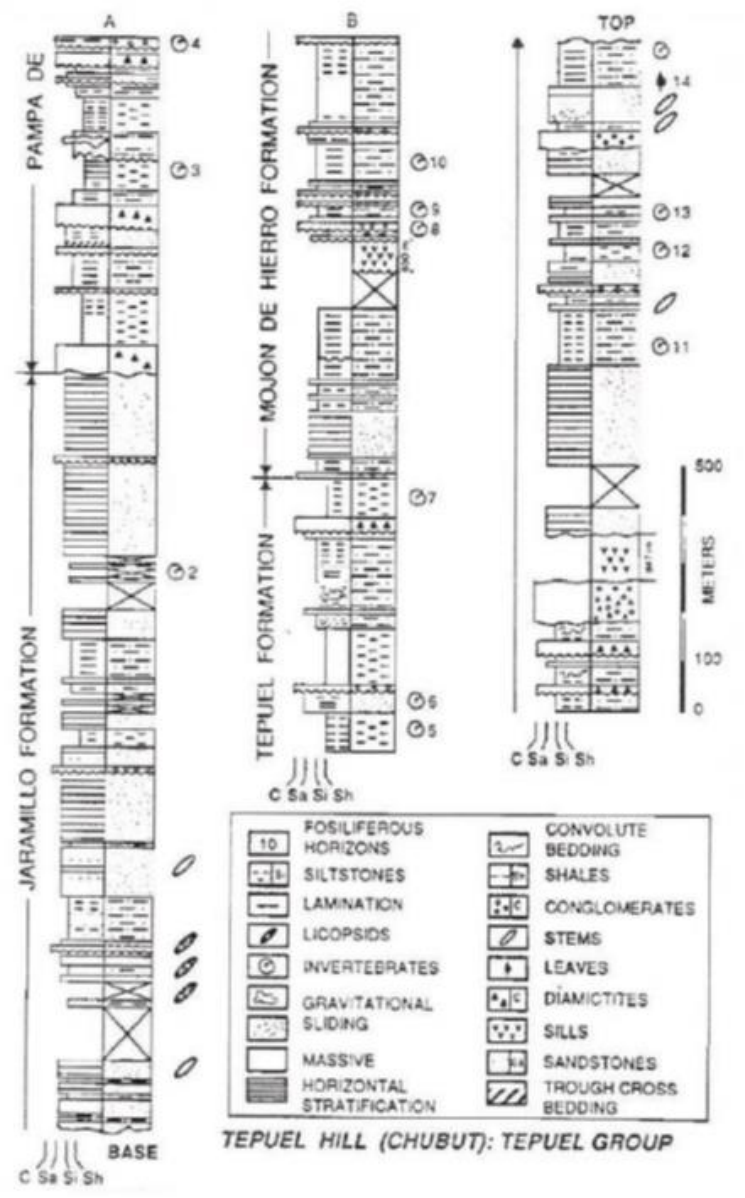

Figure 4. Stratigraphic section from the Tepuel-Genoa Basin containing the Jarmillo, Pampa de Tepuel, and Mojon de Hierro Formations. From Freytes, 1971.

Five diamictite intervals have been identified within the Pampa de Tepuel (Figure 5) (Taboada 2008; 2010). Lopez Gamundi and Limarino (1984) concluded that the diamictites and pebbly mudstones were formed due to debris flows. More recently,

González Bonorino et al, 1988; González Bonorino, 1992; González et al, 1995, González and Díaz Saravia, 2010 concluded that the diamictites formed as a direct result of the presence of glacial ice on the shelf, either in the form of rain-out till or subglacially. Taboada (2008; 2010) interpreted the diamictites as coming from a glacial origin as well. Determining whether or not the diamictite in the field location is of glacial, glaciomarine, or non-glacial origins will help determine the timing and location of glaciation during the LPIA.

Figure 5. Stratigraphic locations of the diamictite units within the Tepuel-Genoa Basin. Modified from Taboada, 2008, 2010; Henry et al., 2012; and Pauls, 2014.

3. Methods

Six stratigraphic sections were measured along a sand body (S43° 42.038, W 70° 43.624) that runs from the north to the south near Tepuel Hill (Figure 6). Sections were measured using standard sedimentological techniques, noting: lithology, grain size, sedimentary structures (especially soft sediment deformation, striated surfaces, and striated clasts), synsedimentary deformation, trace fossils, and the size, shape, and abundance of clasts within different lithologies. This information was used for the lithofacies analysis. Published paleontological data was used to help to constrain the age of these strata.

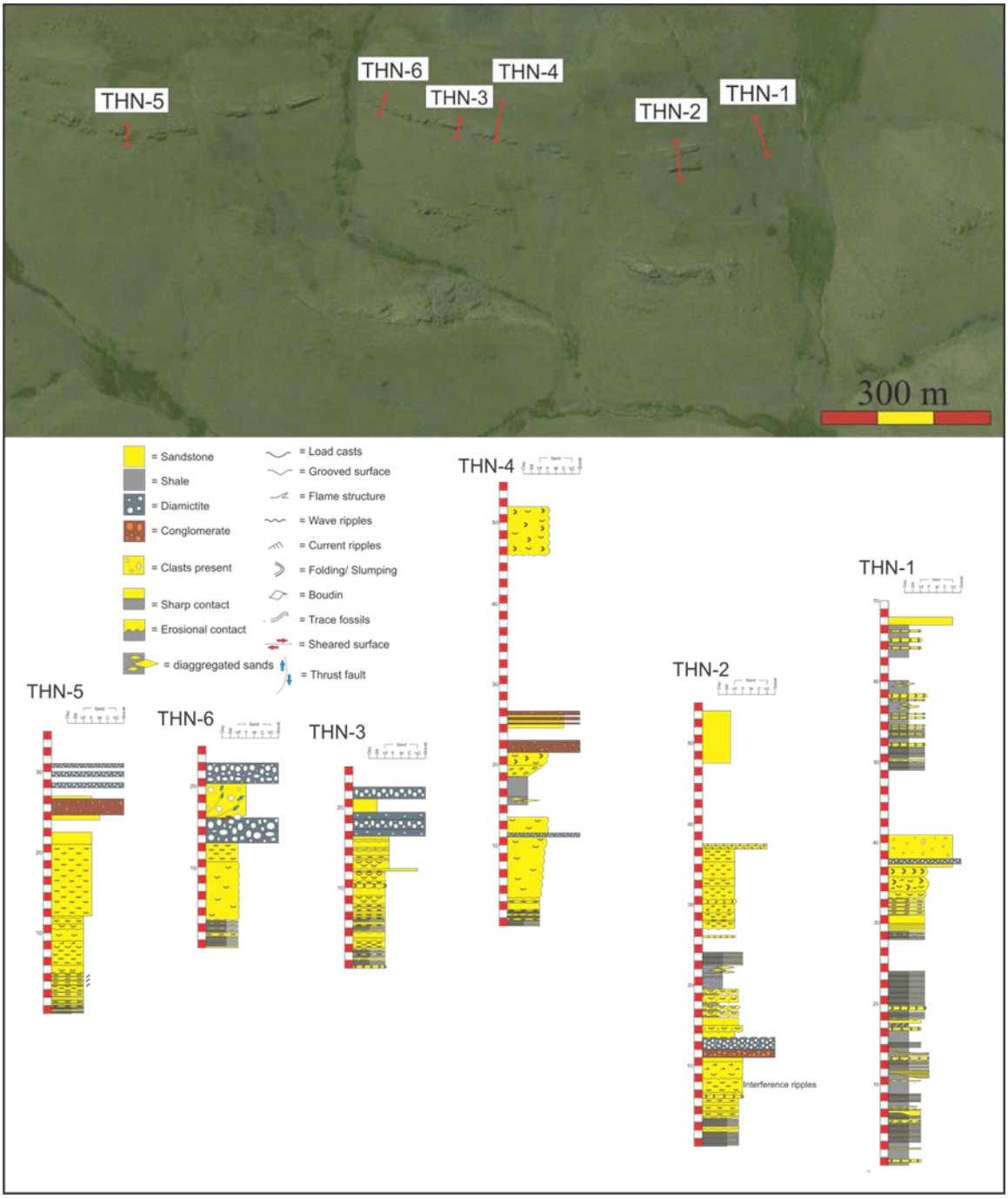

Figure 6. A Google Earth image showing the study site and the locations of the stratigraphic sections along with the stratigraphic columns.

4. Lithofacies Associations

Lithofacies were identified from measured sections logged across a laterally extensive sandstone body that extends across an outcrop face exposed near the head of a valley on the west side of Tepuel Hill. The measured section furthest north was located at S43° 41.450, W70° 43.352, and the section furthest south was located at S43° 42.038, W70° 43.624. The measured strata dip at 35° toward 104°. These strata are divided into eight lithofacies associations which are: 1) massive mudrock 2) thin-bedded sandstone and mudstone, 3) deformed and undeformed sediment blocks, 4) thick-bedded wave-rippled sandstone, 5) large-scale loaded sandstone, 6) conglomerate and massive sands, 7) two diamictite subfacies, and 8) thrust-faulted, massive, boulder-bearing sandstone (Table 1).

Table 1. Lithofacies associations, their descriptions, and their interpreted mechanisms and depositional environments.

Lithofacies Association	Lithologies	Sedimentary Structures	Bed thickness	Interpreted Mechanisms	Depositional Environment
Massive mudrock	Mudstone containing clay and silt	A few clasts present	Mudstone: 1-10's of meters	Settling from suspension	Basinal and slope depostis
Thin-bedded sandstone and mudstone	Mudstone containing clay and silt, very fine to fine grained sandstones	Horizontal laminations, wave ripples present in some sand layers, load structures, flames, folds, trace fossils	Mudstone: 1-15 cm Sandstone: 1-25 cm	Turbidity currents	Marine slope
Large-scale Loaded sandstone	Very fine to fine-grained sandstone	Load structures	Sandstone: .5- 7 m	Seismites, rapid depostion	Marine shelf and slope, tectonically active area
Deformed and undeformed sediment blocks	Very fine to fine-grained sandstone	Folds, boudins, shear planes beneath the slump/slide	Sandstone: .5- 7.5 m	Mass transport down a slope, sediment gravity flows	Marine outer shelf and slope
Thick-bedded, wave-rippled sandstone	Mudstone containing clay and silt; very fine to fine-grained sandstone	Wave and interference ripples, very few, thin mud drapes	Mudstone: 1-2 cm Sandstone: .25-9 m	Wave activity, sand settling out of the water column	shoreface, marine shelf
Conglomerate and Massive Sands	Conglomerate, clast sizes range from 2mm-10cm	Clasts of varying lithologies	Conglomerate: .25-2 m	Debris flows	Marine shelf and slope
Diamictite subfacies 1	Massive, clast sizes range from 5cm-25 cm	Clasts of varying lithologies	Diamictite: .5- 1.5 m	Debris flows	Marine shelf and slope
Diamictite subfacies 2	Massive, clast sizes range from 5 cm- 75 cm	Clasts of varying lithologies, striated clasts	Diamictite: 2- 3.5 m	Plume settling and ice rafted debris	Near the glacial margin, marine shelf
Massive, boulder-bearing sandstone	Fine-grained sandstone, pebbles, cobbles, and boulders present	Folding, thrust-faults, granite clasts	Sandstone: 4 m	Glacial-shoving of sediment	Near the glacial margin, marine shelf

4.1 Mudrock Facies

Description

The mudrock facies occurs both above and below the strata described in each of the measured sections (Figure 7). This facies makes up the greatest thickness of sediment exposed in the Tepuel Hills. It forms the thick bases of repetitive, coarsening-upward mudrock to coarse-grained clastic successions exposed throughout the range. The base of these mudstones are in sharp contact with coarse clastics at the top of underlying successions, and near the top of the succession, this facies grades into interbedded sand and mud deposits. The mudstone portion of these successions is typically 10's to hundreds of meters thick. Isolated blocks of deformed sandstone and undeformed sandstones resting on shear planes occur scattered throughout this lithofacies (see deformed and undeformed sediment blocks facies). Mudrocks that occur directly below the measured sections in this study contain invertebrate fossils associated with the *Lanipustula* biozone (Pagani and Taboada, 2010; Pauls, 2014). Within the studied strata, this facies was measured in part in sections THN-1, THN-2, and THN-4 and ranges from 1 to 10's of meters in thickness within the measured sections. However, it should be noted that the entire thickness of the lithofacies was not measured during this study. This facies is made up of a mixture of clay and silt, with rare lonestones (Figure 8) and bullet-shaped, striated clasts ranging from 2 to 25 cm in diameter. In the mudstone facies contained within THN-2, the frequency of the lonestones decreases up section toward the thick, laterally continuous, wave-rippled sandstone.

Figure 7. Google Earth image showing the massive mudrock facies present throughout most of the study location surrounding the sand body.

Figure 8. Lonestone-bearing mudstone made up of silt and clay located in section THN-2 within the Pampa de Tepuel Formation. Hammer for scale.

Interpretation

Mudrocks within the measured sections were deposited as silt, mud, and clay that settled from suspension as hemipelagic deposits (Isbell et al., 2011, 2013b; Pauls, 2014). These units are marine in origin as indicated by the presence of marine fossils (Pagani and Taboada, 2010; Pauls, 2014). The thickness of the mudrocks within the coarsening upward successions, and an absence of sedimentary structures produced by wave activity suggest deposition in relatively deep water well below storm wave base. Such thicknesses of 100s of meters suggest that these strata were deposited on marine slopes beyond the shelf-slope break. The presence of bullet-shaped clasts and lonestones within this facies indicate a possible origin of the clasts as ice-rafted debris. The shape of the clasts and the presence of striations suggest that they were rafted by icebergs rather than by sea ice (cf. Thomas and Connell, 1985; Gilbert, 1990; Carto and Eyles, 2012; Pauls, 2014).

4.2 Thin-bedded sandstone and mudstone facies

Description

The thin-bedded sandstone and mudstone lithofacies occurs in all of the measured sections, but are most common in THN-1. This facies ranges up to 6 meters in thickness. The lithologies that make up this facies include laminations and thin beds (mm to cm scale) of alternating mudstone and very fine to fine-grained sandstone (Figure 9). Stratification consists of alternating horizontal laminations of mudstone and sandstone that range from millimeters to a couple of centimeters thick. Current ripples appear in some of the sand layers (Figure 10) while trace fossils are present in some of the mud

layers. Small-scale (cm scale) soft sediment deformation such as load casts, flame structures, and recumbent folds occur sporadically throughout the facies (Figure 11).

Figure 9. Alternating mudstone and fine-grained sandstone beds located in section THN-1 within the Pampa de Tepuel Formation. Units on the scale are in mm.

Figure 10. Current ripples present within the alternating fine-grained sandstone and mudstone beds located in section THN-1 in the Pampa de Tepuel Formation. Units on the scale are in mm.

Figure 11. Dewatering features in alternating fine-grained sandstone and mudstone located in section THN-1 within the Pampa de Tepuel formation. Units on the scale are in mm.

Interpretation

The thin-bedded sandstone and mudstone facies is interpreted as having been deposited incrementally by turbidity currents. Folded units are interpreted as small slumps, and load and flame structures suggest the presence of water saturated sediments and water escape from the sediments. Larger slump and slide structures are described in the deformed sediment facies. Active slides and slumps often transition into linked debris flows and turbidity currents as water is incorporated into the deforming mass and then sediment is stripped from the resulting debris flow (Hampton, 1972; Haughton et al., 2003; Amy and Talling, 2006; Talling et al., 2007, 2012).

The alternating laminae of sand and mud represents episodic production of density currents and coincides with the description of a turbidite (Hampton, 1972; Mulder and Alexander, 2001; Haughton et al., 2003, 2009; Sumner et al., 2012; Talling et al., 2007, 2012). If bedforms are formed, it is believed that the flow was a lower density flow. A lower density flow would have more turbulent water closer to the bed because there is less sediment in suspension, allowing for the formation of bedforms including planar laminations (Mulder and Alexander, 2001; Haughton et al., 2003; Sumner et al., 2012; Talling et al., 2012). The opposite would be true for higher density turbidity currents. Because there are higher sediment concentrations closer to the bed in high density turbidity currents, the water will be less turbulent near the beds hindering the formation of bedforms, which results in massive sand deposits (Talling et al., 2012).

Some soft sediment deformation was observed within the thin-bedded sandstone and mudstone facies in the study area. Small scale soft sediment deformation is likely to

occur within a turbidite, in intervals containing fine sands and current ripples (Haughton et al., 2003, 2009; Mulder and Alexander, 2001; Talling et al., 2012). It is thought that the fine-grained sand that makes up the rippled interval has a low permeability creating small-scale water escape and load structures as fluid trapped during deposition escapes upward toward the sediment water interface (Haughton et al., 2003, 2009; Talling et al., 2012).

4.3 Deformed and undeformed sediment blocks facies

Description

Deformed and undeformed sediment blocks (Figure 12) occur in sections THN-1, THN-2, and THN-4 of the measured sections. This facies is comprised of very fine to fine-grained sandstone and contain large-scale folds up to 2 m thick (Figures 13 and 14) and disaggregated sandstone bodies (up to 1 m thick and 2 m wide) surrounded by mud. Boudins and sheared horizons are present at the base of the blocks in some areas (Figures 15 and 16). There are deformed blocks of folded sandstone that are stacked on top of each other in section THN-1. These blocks only occur to the south of section THN-4 or are contained within the thick overlying and underlying mudrock facies. If the blocks are traced laterally south, they start to become disaggregated (Figure 17). The underlying sediment displays evidence of having been sheared, and in some places grooved and striated surfaces occur directly beneath the deformed sandstone blocks.

Figure 12. Fine-grained sandstone stacked slide and slump blocks located in section THN-1 within the Pampa de Tepuel Formation. Jacob's staff for scale.

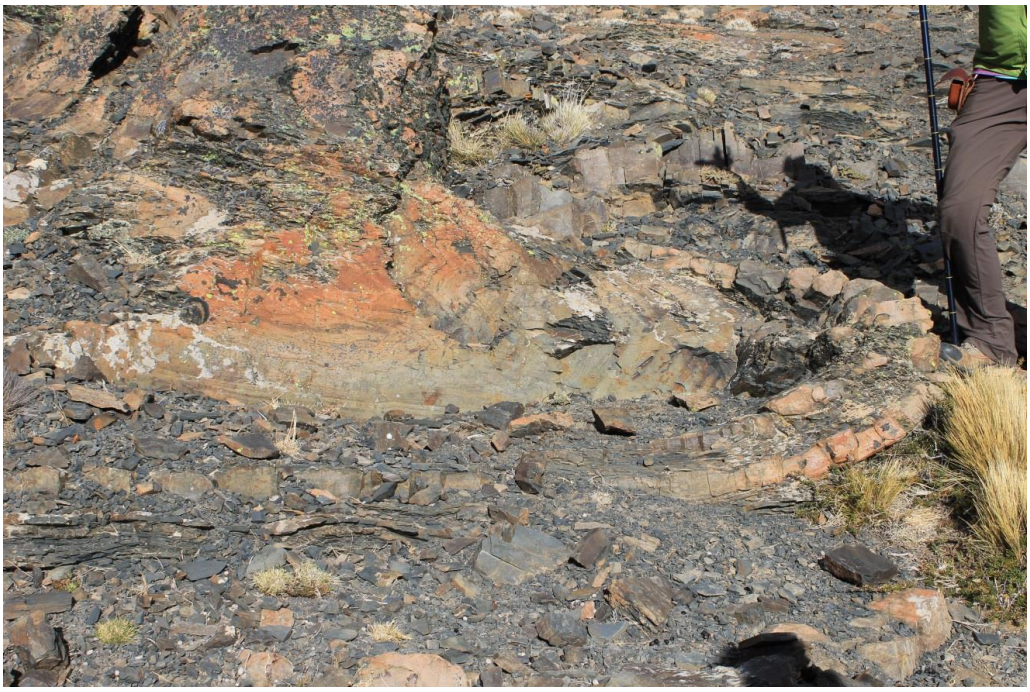

Figure 13. Fold within a slumped block of fine-grained sandstone with some mudstone located in section THN-4 within the Pampa de Tepuel Formation. Person for scale.

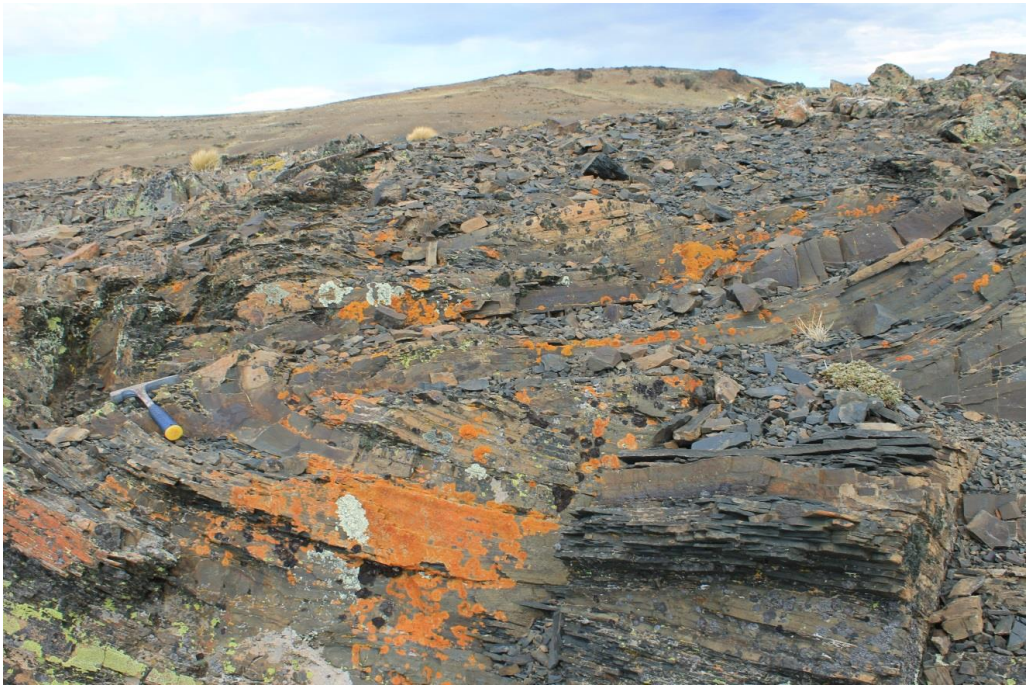

Figure 14. Fold within a slumped block of fine-grained sandstone and mudstone located in section THN-4 within the Pampa de Tepuel Formation. Hammer for scale.

Figure 15. Sheared plane located beneath a slumped block in section THN-4 within the Pampa de Tepuel Formation. Hammer for scale.

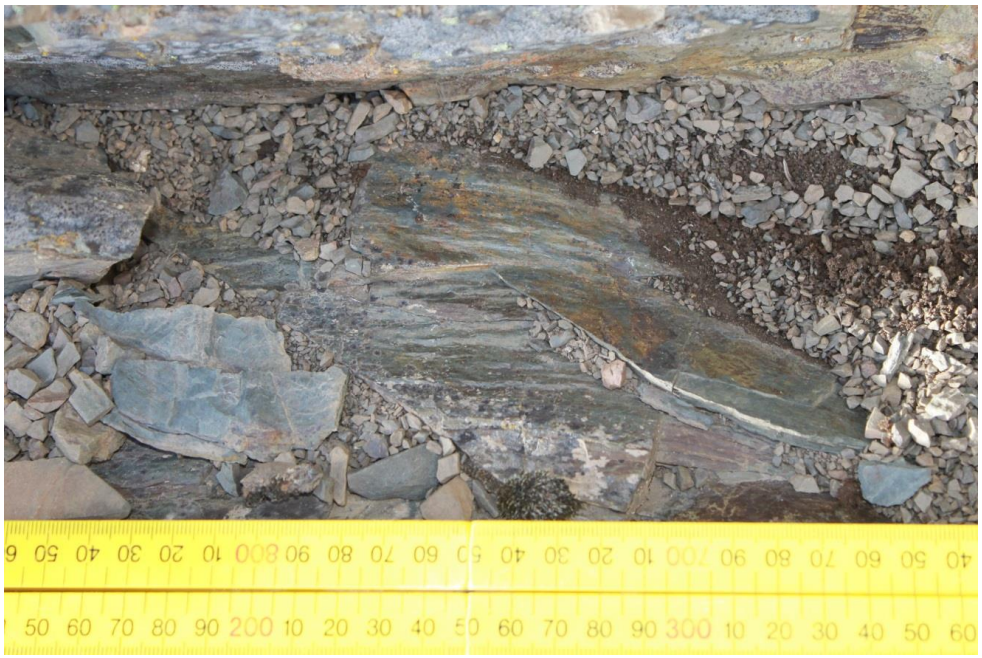

Figure 16. Sheared plane on mudstone located beneath a slide block in section THN-1 within the Pampa de Tepuel Formation. Units on the scale are in mm.

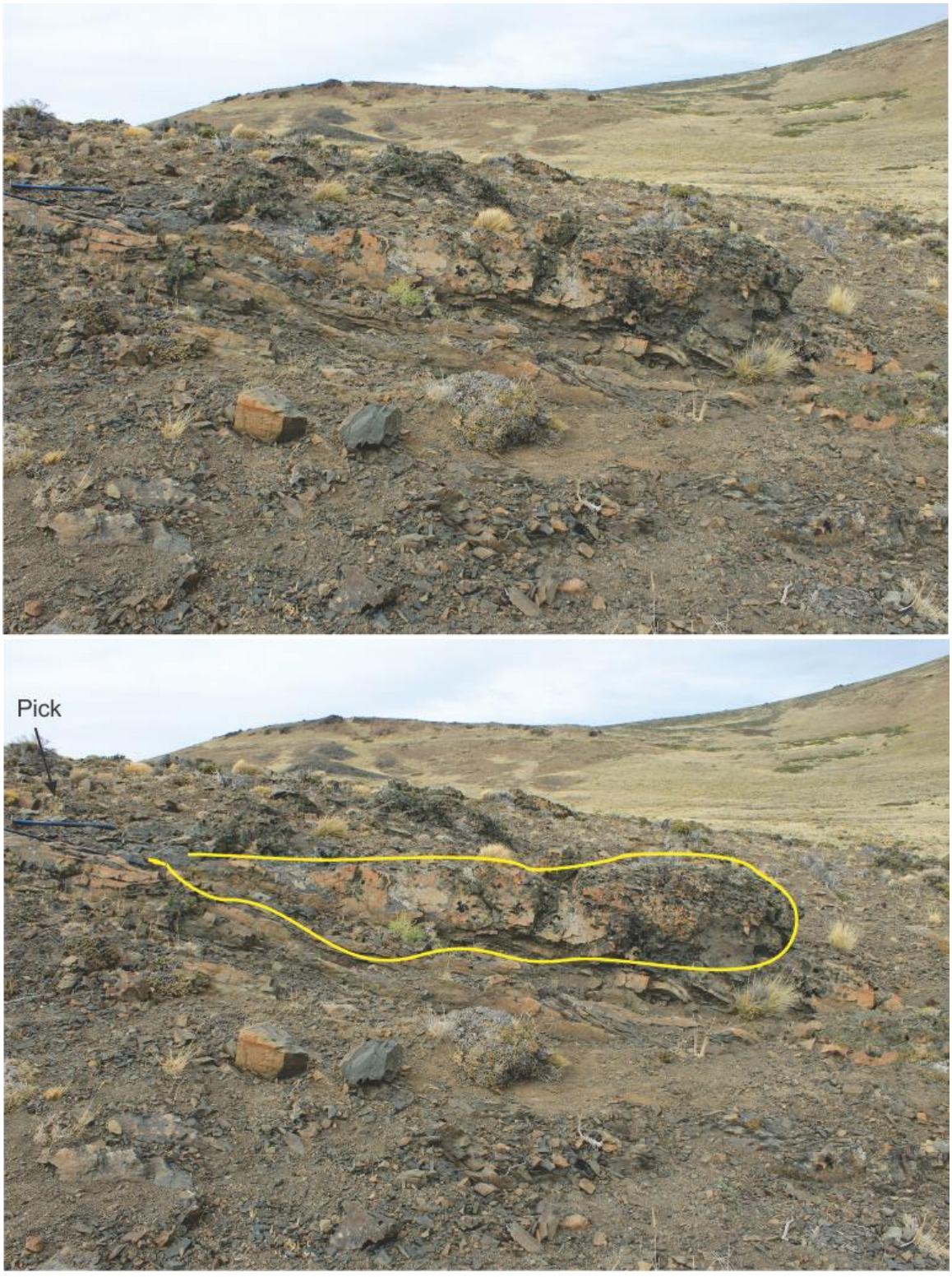

Figure 17. Dissaggregated body of fine-grained sandstone surrounded by mudrock located in section THN-1 within the Pampa de Tepuel Formation. Pick for scale.

Interpretation

The deformed and undeformed sediment blocks are interpreted to be slide and slump blocks respectively that formed from mass movement on an unstable surface. The interpretation is based on the presence of boudins and sheared horizons beneath the blocks of sand and on either the internal deformation or the anamolous occurrence of blocks of sandstone surrounded by mudrock. The folding is also contained within the sand blocks, with no folding occurring in the units above or below, indicating that it is part of the soft sediment deformation and not caused from a large scale tectonic folding event (Smith, 2000; Strachan, 2002; 2008; Posamentier and Walker, 2006; Lee et al., 2007; Callot et al., 2009; Van Der Merwe et al., 2011).

The sliding and slumping could have been caused by over loading of sediment on a slope or due to seismic activity. Failures along a slope can be caused by many factors including high sedimentation rates, the angle of the slope, a rise or fall of relative sea level, and seismicity (Lee et al., 2007). Even with low angle slopes, if sediment is rapidly loaded and has a low permeability, the excess pore pressure can cause a reduction of the effective shear strength of the underlying mud leading to a slide which can become a slump as the sediment begins to accelerate and deform as more fluid is incorporated into the flow (Bryn et al., 2005; Lee et al., 2007; Strachan, 2008). A glide plane develops on the mud as the block slides downslope causing shearing, boudinage, and the development of a grooved surface, which is what is seen in some areas. Boudinage structures could occur as some of the lower sand is pulled apart as sliding occurs. The sediment block can continue to transform during sliding by the disaggregation of the sand bodies and eventually become a debris flow and/or turbidity current (Strachan, 2008).

This would explain the origin of turbidites located stratigraphically below the slide and slump block facies. These deposits would typically be found on basinal slopes beyond the shelf slope break.

4.4 Thick-bedded, wave-rippled sandstone facies

Description

The thick-bedded wave rippled sandstone lithofacies occurs mainly in measured sections THN-5, and THN-6 and ranges in thickness from 1 -9 m. It is made up of very fine to fine-grained sandstone displaying symmetrical ripples and wave-ripple cross laminations (Figures 18 and 19), and in some area, interference ripples (Figure 20). Rare, thin mud drapes occur on some of the ripples near the base of the facies and these drapes have trace fossils present on the surface (Figure 21). Within this facies, sandstone coarsens upward from very-fine to fine sandstone. Directly below this facies is the thin-bedded sandstone and mudstone facies with a relatively sharp transition into the wave-rippled sandstone with no hummocky cross beds present in between. Directly above this facies are diamictite and mudrock deposits.

This facies is also present within a 6 m section of THN- 2 located South of THN-5 and THN-6. The sand ranges in grain size from very fine to coarse, and there is a coarsening upward sequence with the ripples becoming asymmetric up section as the sand coarsens. Below this facies are mudrock and thin bedded sandstone and mudstone deposits, and above this facies is a thick mudrock succession.

Figure 18. Wave-rippled, fine-grained sandstone bed located between sections THN-5 and THN-6 within the Pampa de Tepuel Formation.

Figure 19. Wave-rippled, fine-grained, sandstone bed located in section THN-5 within the Pampa de Tepuel Formation. Units on scale are in mm.

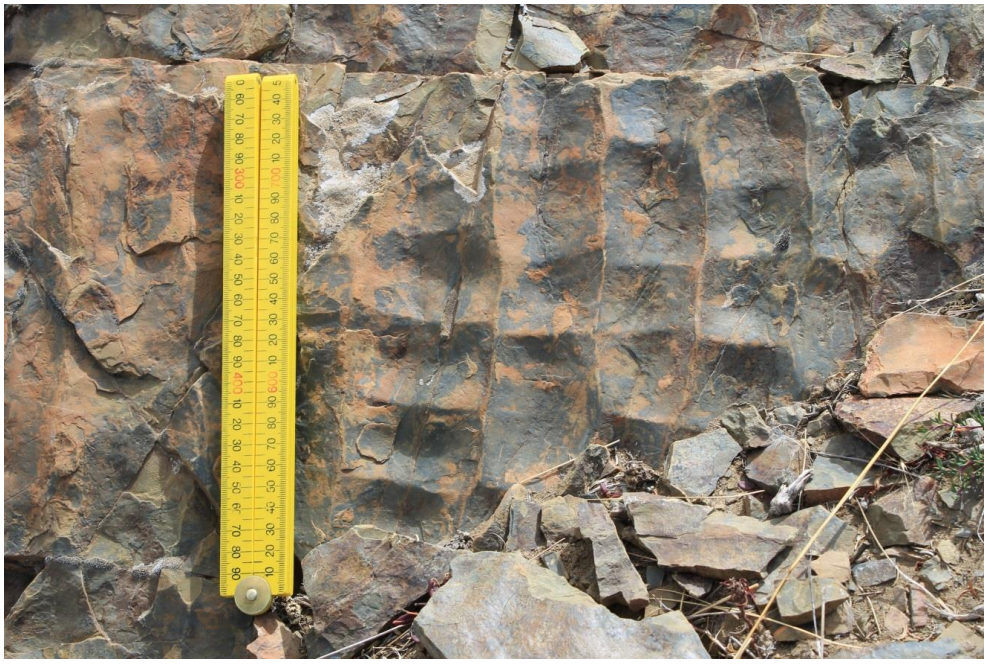

Figure 20. Interference ripples in fine-grained sandstone located between sections THN-5 and THN-6 within the Pampa de Tepuel Formation. Units of scale are in mm.

Figure 21. Thin mud drape containing trace fossils on fine-grained rippled sandstone located in section THN-5 within the Pampa de Tepuel Formation. Units on scale are in mm.

Interpretation

The thick-bedded, wave-rippled sandstone facies is interpreted to be part of a shoreface deposit. In shoreface deposits, sediment coarsens upward as part of a shallowing upward succession and contains abundant wave generated sedimentary structures including ripples (Clifton, 2006; Hampson et al., 2008; Plint, 2010; Varkarelov et al., 2012). The abundance of wave-rippled sandstone and an absence of mud deposits, except for rare mud drapes at the very base of the succession, indicate deposition above normal wave base (Clifton, 2006; Hampson et al., 2008; Plint, 2010; Varkarelov et al., 2012).

An abrupt transition does occur between the thin-bedded sandstone and mudstone facies and the wave-rippled sandstone facies. The thin-bedded sandstone and mudstone facies is typical of deeper water deposits below storm wave base and transitions quickly to the wave-rippled sandstone which would have been deposited above normal wave base. The transition zone containing hummocky cross beds that would be present in a normal shoreface succession is missing. This could be the result of an abrupt drop in relative sea level or a forced regression that caused deposits from above normal wave base to be deposited on top of deeper water deposits as relative sea level dropped rapidly (Plint, 1988; Clifton, 2006; Plint, 2010). This could also be due to sea ice blocking storm wave activity from occurring (Lisitzin, 2002), but this seems less likely as it would have also impacted wave activity including that above normal wave base.

4.5 Large-scale loaded sandstone facies

Description

Loading is common within the deformed facies and is located in all of the measured sections. The loaded sections are made up of very fine to fine-grained sandstone and contain large-scale load structures with widths up to 10 m and thicknesses up to several meters, which are loaded into underlying wave-rippled sandstones. Load structures occur entirely within the sandstone succession. The structures may be entirely massive internally or retain relic deformed bedding. Between the large loads, flames or diapirs of sandstone extend up to 3 meters vertically (figure 22). These loads occur in laterally and vertically extensive zones of overlapping load structures up to 100 meters wide and up to 10 meters thick (Figures 23, 24, and 25). The loading is contained within and surrounded by the thick-bedded wave-rippled sandstone facies which has a grain size of very fine to fine-grained sand. In a few places, undeformed, wave-rippled sandstones occur within zones of extensively loaded sandstone.

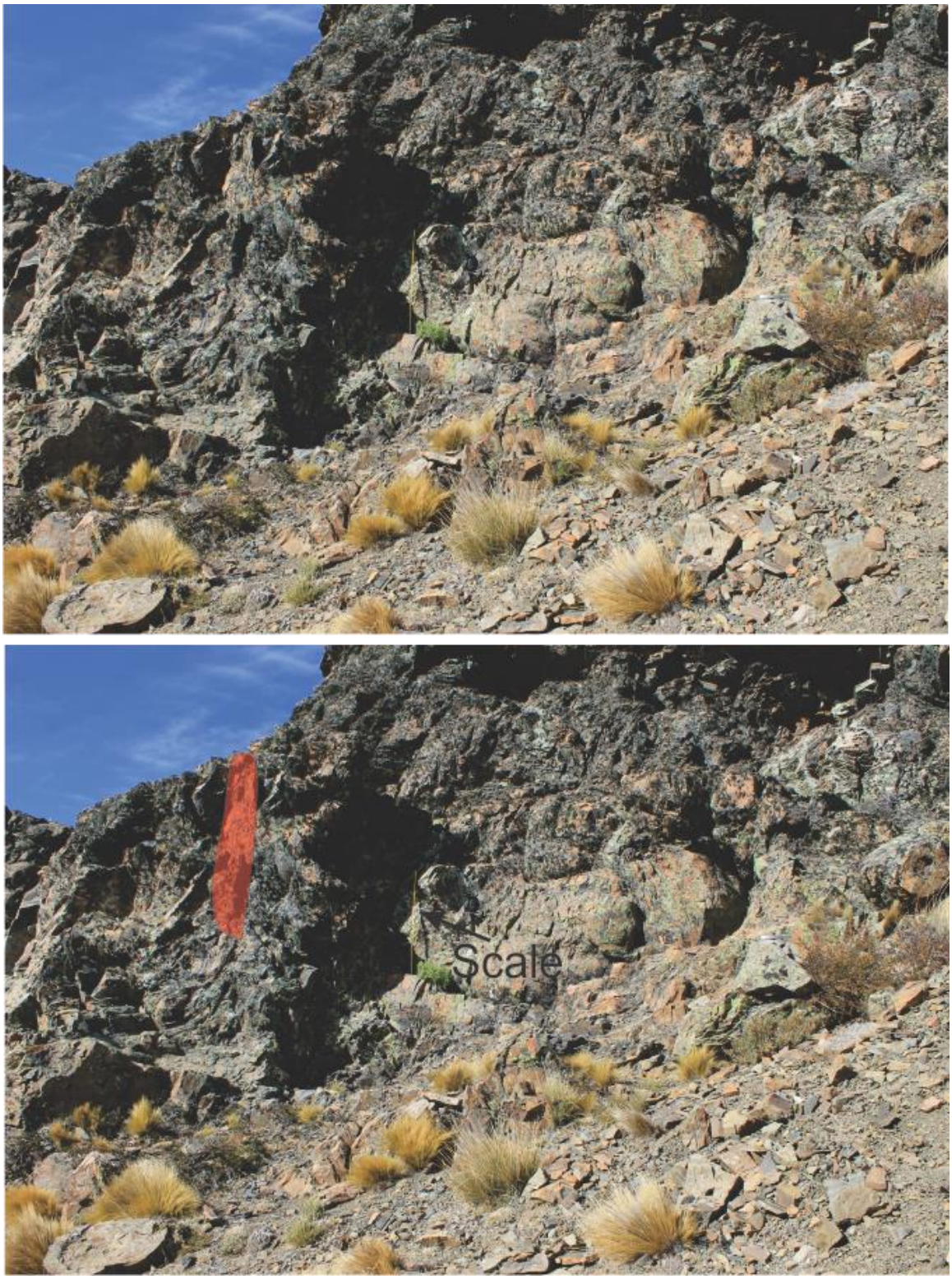

Figure 22. Fine-grained sand diaper located in the loaded facies in section THN-3 within the Pampa de Tepuel Formation. The diaper is highlighted in red. Scale is 1 m.

Figure 23. Large-scale loaded sections made up of fine-grained sandstone located in section THN-3 within the Pampa de Tepuel Formation. The white dashed line shows the lower boundary of the section and the yellow lines show the stacked loads with the loaded section. Person for scale.

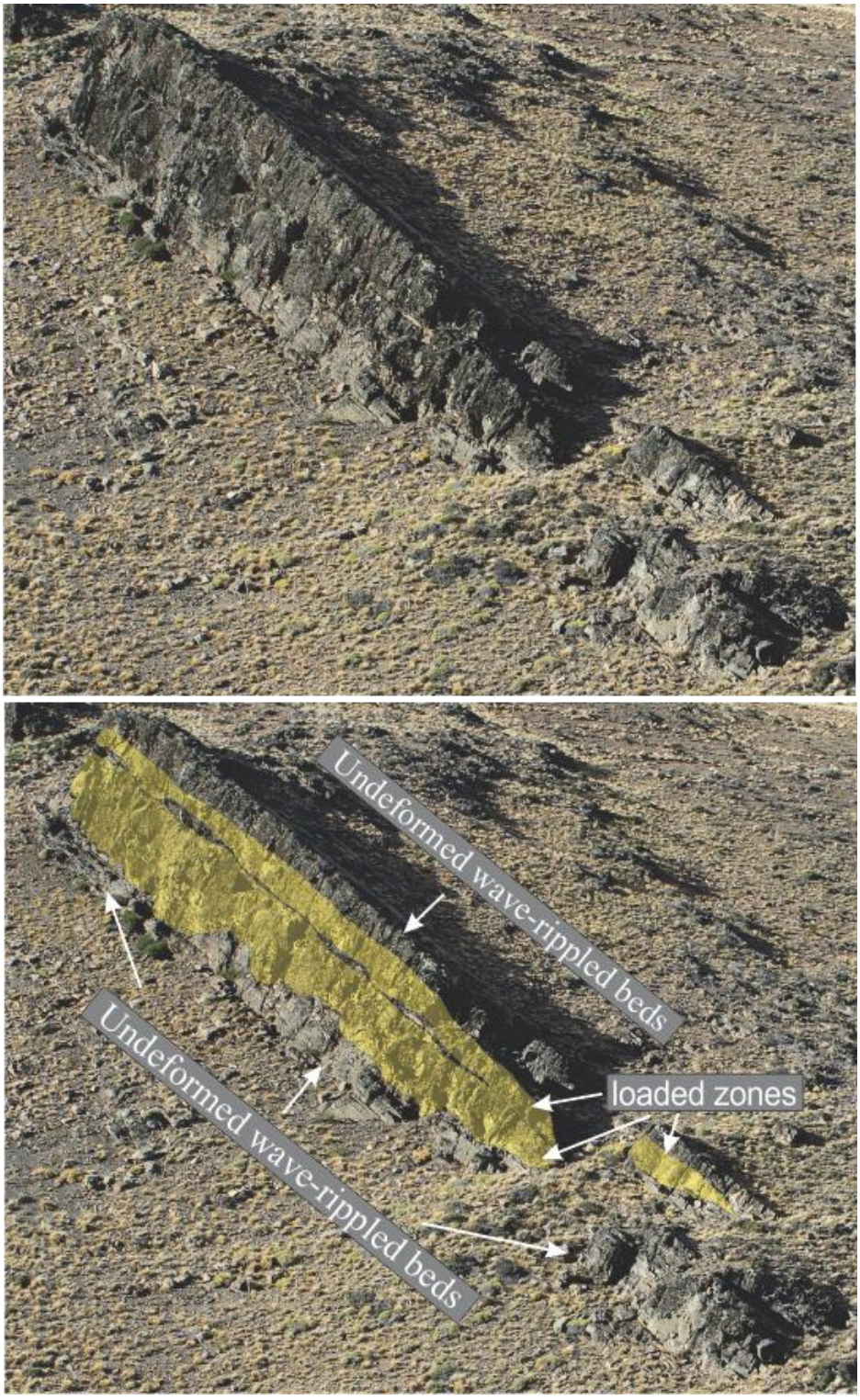

Figure 24. Large-scale loaded fine-grained sandstone with the loaded zones highlighted in yellow. This area is located between THN-5 and THN-6 within the Pampa de Tepuel Formation. Loaded zone is about 100 m wide.

Figure 25. Fine-grained sandstone load structure located between THN-3 and THN-6 within the Pampa de Tepuel Formation. Person for scale.

Interpretation

Load structures are rounded or irregular shaped lobes that form on marine shelves or slopes or in areas where the sediment is highly water saturated. These structures can be formed due to liquefaction because of a shock applied to the unconsolidated sediment or due to rapid sedimentation that creates excess pore-fluid pressure and causes the sediment to sink into an underlying layer as the water escapes (Allen, 1984; Mulder and Alexander, 2001; Collinson et al., 2006). Load structures that form due to rapid sedimentation are generally small-scale and can be found in shallow water caused by storm waves and associated rapid sedimentation events (Mulder and Alexander, 2001), but they are more common in deeper water deposits such as turbidites (Haughton et al., 2003). With liquefaction, fine sands are most susceptible to loading and deformation (Montenat et al., 2007), and the internal bedding is usually destroyed (Collinson et al., 2006). This type of load is referred to as a seismites. With seismites, it is common to have long (up to several meter) diapirs of fine sand cutting between m-scale load structures (Montenat et al., 2007).

It can be difficult to differentiate seismites from loading caused by other processes such as rapid deposition due to sediment gravity flows because many of the indicators are the same (Bezerra et al., 2001; Greb et al., 2002; Montenat et. al., 2007; Ettensohn et. al., 2011). Greb et al. (2002) and Ettensohn et al. (2011) put forth criteria that can help to differentiate seismites from other forms of soft-sediment deformation which includes: 1) deformation occurring within a seismically active basin, 2) deformation that is widespread regionally, 3) deformation that can be stratigraphically constrained regionally, and 4) deformation that shows increases in size, frequency or

intensity of deformation towards a likely epicentral area. The large-scale loading across the sand bodies for this study were constrained stratigraphically and were widespread across the outcrop. The loads in the area are massive but are stratigraphically surrounded by wave-rippled sandstones interpreted to be part of a shoreface succession. Hummocky stratification deposits, which suggest deposition from intense storm activity, were absent within the study area, so it is unlikely that the loading was caused by rapid depositions of storm-wave sediment on the shelf. Long diapirs of fine sand were also present within this section. Therefore, the load structures in the study area are interpreted to be seismites that formed due to tectonic activity that occurred after deposition (Bezerra et al., 2001; Greb et al., 2002; Montenat et al., 2007; Ettensohn et al., 2011; Wallace and Eyles, 2015).

4.6 Conglomerate and Massive Sands facies

Description

Conglomerates and massive sands appear in sections THN-2, THN-4, and THN-5. They range in thickness from 0.5 m to 2 m. The conglomerates are made up of clasts of varying lithologies including granite, sandstone, and shale, and range in size from 2 mm - 10 cm in diameter. Small amounts of mud occur in the matrix. The conglomerates generally appear alternating with massive sands that show no internal structures (Figure 26). In THN-4 the conglomerate contains a lot of very coarse sand, and is interbedded with very coarse sand (Figure 27). The sands range in grain size from fine to coarse, and the thickness of the sections range from about .25m to 2 m. Some of the massive sands contain pebbles and a few cobbles.

Figure 26. Alternating massive sandstone and conglomerate. Conglomerate contains quartzite and sandstone clasts and the massive sandstone is coarse-grained. From section THN-4 within the Pampa de Tepuel Formation. Hammer for scale.

Figure 27. Coarse-grained sandstone containing some small pebbles located in section THN-1 within the Pampa de Tepuel Formation. Hammer for scale.

Interpretation

The conglomerate and massive sand facies is interpreted to have formed from a grain flow or turbidity current. The massive sands and conglomerates were most likely part of a sandy turbidity current, and because the conglomerate beds are relatively thin, they were probably left behind by the main part of the flow (Posamentier and Walker, 2006; Talling et al., 2012). It can be difficult to tell the difference between sand deposited from a debris flow or from a turbidity current, but an indicator that the sand was deposited by a turbidity current is that if clasts are present, they are generally aligned in a single horizon (Talling et al., 2012). The sands were almost always found with a thin

conglomerate layer beneath them indicating that the flow was most likely a turbidity current. Very few large-scale experiments have been performed on conglomerates, so the interpretation remains somewhat speculative as well (Posamentier and Walker, 2006).**4.7 Diamictite facies**

Two distinct diamictite facies were identified within the study section. Both were massive and contained clasts of sandstone, granite, and shale with no preferred fabric, but differences in thickness, surrounding facies, and clast abundances lead to different interpretations. They are separated into two subfacies described and interpreted below.

Diamictite subfacies 1

Description

The first is located to the south of column THN-4. It is massive and also has no preferred fabric (Figure 28). This diamictite is less than 2 meters in thickness and was found in proximity to the deformed and undeformed sediment blocks facies, the thin-bedded sandstone and mudstone facies, and the conglomerate and massive sandstone facies (Figure 29). The clasts in this diamictite are smaller (less than 20 cm), and less abundant than the diamictite present to the north of THN-4.

Figure 28. Massive diamictite with clasts of sandstone and quartzite located in section THN-1 within the Pampa de Tepuel Formation. Units on scale are in mm.

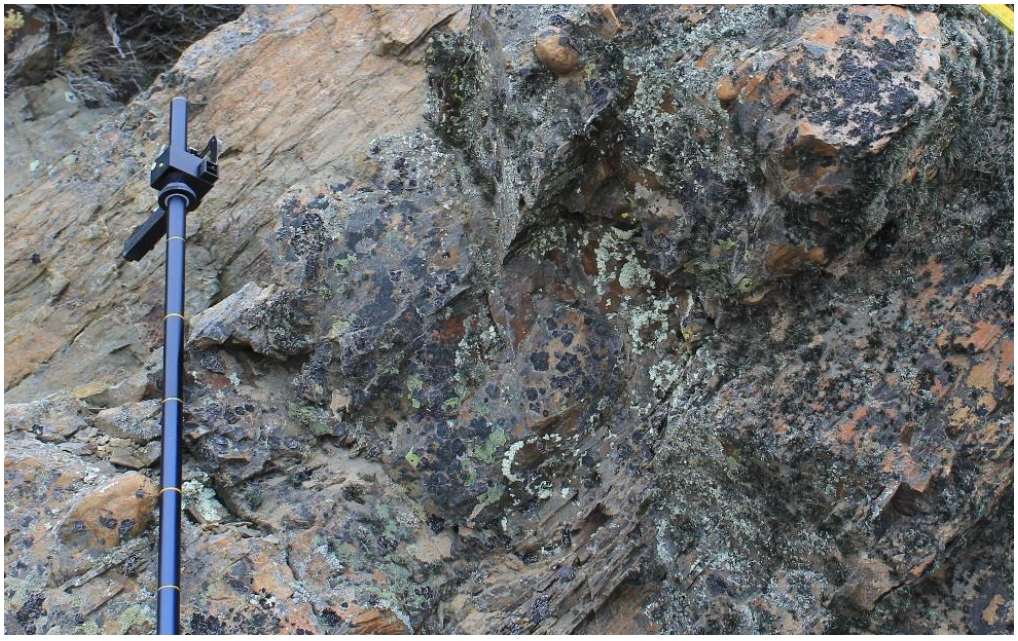

Figure 29. Massive diamictite with sandstone and granite clasts located in section THN-2 within the Pampa de Tepuel Formation. Jacob's staff for scale.

Interpretation

The proximity of the diamictite facies located to the south of THN-4 to the deformed and undeformed sediment blocks facies, thin-bedded sandstone and mudstone facies, and the conglomerate and massive sandstone facies along with a thickness of less than 2 meters suggests that this diamictite facies was deposited by debris flows. Moderate-strength debris flows would leave deposits that are generally less than 2 meters thick (Talling et al., 2004, 2012), which is what is present in THN-1, THN-2, and THN-4. The slide and slumped blocks and turbidity current deposits are commonly found in proximity to diamictites because during failure events, flow types can transform (Figure 30) as mixing of water and debris occurs (Carto and Eyles, 2012). The moderate-strength debris flows are more likely to generate turbidites because they are more prone to mixing (Talling et al., 2012), and turbidite deposits are abundant within and around these three stratigraphic columns.

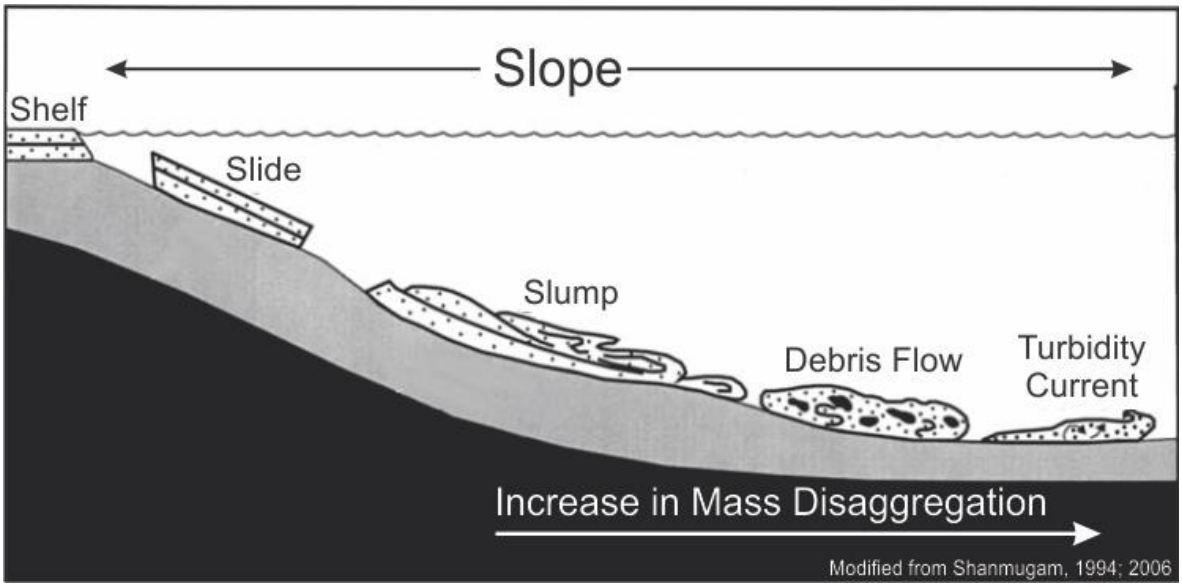

Figure 30. Diagram showing the transformation from slide and slump blocks into debris flows and turbidity currents. Modified from Shanmugam 1994, 2006.

Diamictite subfacies 2

Description

The second diamictite facies found in sections THN-3, THN-5, and THN-6 are thicker (2-3 meters) and contain larger (up to .5 m) clasts that are found in clusters in some areas and are less abundant in other areas (Figure 31). Some of the clasts within this diamictite display striations (Figure 32). Below this facies is the thick-bedded wave-rippled sandstone facies. In THN-6 the massive, boulder-bearing sandstone facies is stratigraphically constrained by this facies. The diamictite beneath the massive, boulder-bearing sandstone facies is sheared along its upper surface (Figure 33) but it is only sheared when the thrust- faulted, massive, boulder-bearing sandstone facies is above it. When traced laterally to the South, the diamictite thins and pinches out.

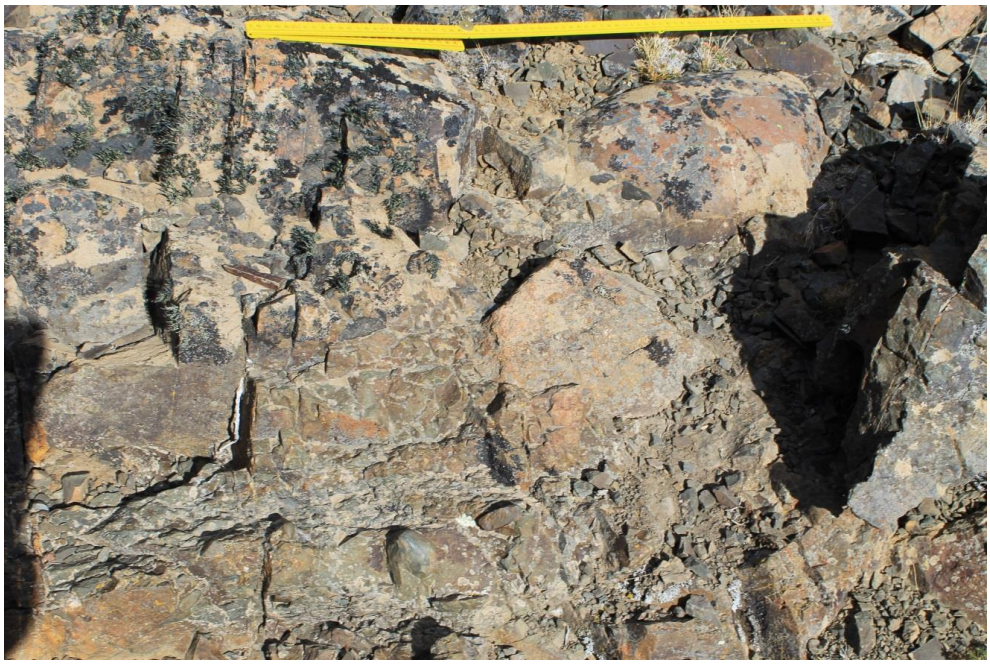

Figure 31. Diamictite containing large clasts of granite, sandstone, and shale located in section THN-6 within the Pampa de Tepuel formation. Units on scale are in mm.

Figure 32. Striated clast within a massive diamictite located near section THN-3 within the Pampa de Tepuel Formation. Clast has about a 2 cm diameter.

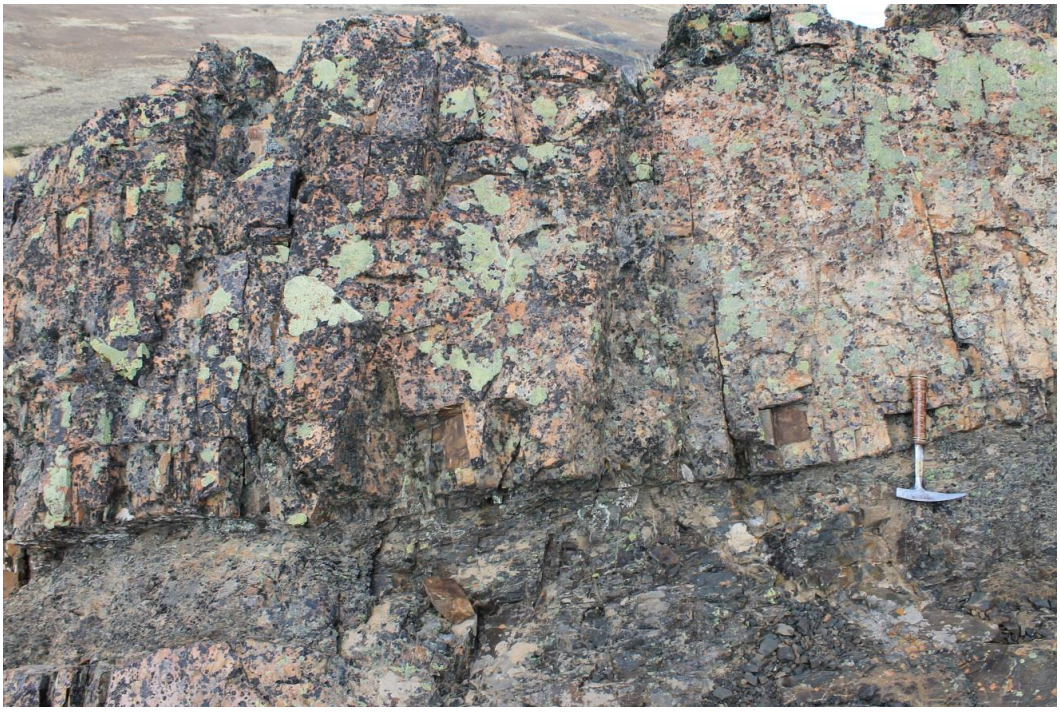

Figure 33. Sheared top of diamictite below the massive, boulder-bearing sandstone facies located near section THN-6 within the Pampa de Tepuel Formation. Hammer for scale.

Interpretation

In glaciomarine environments, massive diamictites can form from rain out of debris from melting ice, debris flows, or from basal melting that releases debris near the grounding line (Eyles et al., 1983; Eyles et al., 1985; Cowan and Powell, 1990; Hambrey et al., 1991; Dowdeswell et al., 1994). The presence of striated clasts within the diamictite suggests a glacigenic origin, and the discontinuous clustering and size of the clast suggests that they could be due to rain-out from icebergs (Powell and Cooper, 2002), possibly as dump structures. The thickness of the mud and the location of the mud above the fine sands suggests that they were deposited as rainout of fine-grained material from a meltwater plume (Powell and Domack, 2002). The massive diamictite deposits that are present in columns THN-3, THN-5, and THN-6 were most likely formed from rain out of mud and fine-grained material from a melt-water plume from a nearby glacier and/or melt out of material directly from glacial ice and icebergs (Cowan and Powell, 1990; Isbell et al., 2008a).

4.8 Thrust faulted, Massive, boulder-bearing sandstone facies

Description

The thrust-faulted, massive, boulder-bearing sandstone facies occurs in THN-6 between 16 m and 20 m above the base of the section (Figure 34). It is comprised of fine-grained sandstone that contains scattered granite clasts ranging in size up to .5 meters in diameter (Figure 35). The unit is massive and no internal bedding was noticed within this facies. However, this unit is cut by multiple, listric-shaped thrust-faultsthat extend from the base to the top of the sandstone body over a distance of several 10's of

meters. The faults are lined by centimeter thick zones of sheared sediments. In at least one place along the exposure, stacking of thrust sheets occurs, and the sheets form a series of back-stepping thrust blocks. The faults do not cut either underlying or overlying sedimentary deposits. The top of the diamictite facies directly below this facies is sheared. However, the diamictite above this facies is undeformed. The sandstone body is wedge shaped and when traced laterally to the south, the sandstone unit pinches out with no fold nose present.

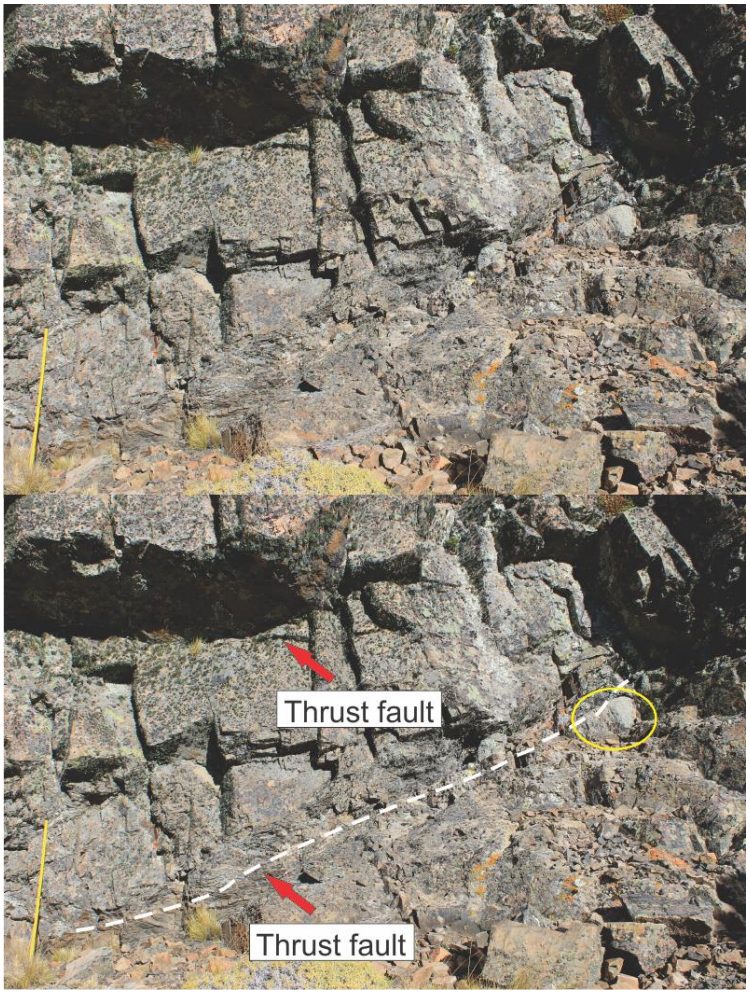

Figure 34. Boulder-bearing, fine-grained sandstone containing listric-shaped thrust faults located in section THN-6 within the Pampa de Tepuel Formation. The white dashed line shows the sheared diamictite below the facies. A large granite boulder is circled in yellow. Scale is 1 meter high.

Figure 35. Granite boulder contained within the faulted fine-grained sandstone located in section THN-6 within the Pampa de Tepuel Formation. Units on the scale are in mm.

Interpretation

The massive, boulder-bearing sandstone facies was formed due to compressive forces. This is suggested by the occurrence of listric-shaped thrust faults. Compression in syn-depositional settings is the result of either frictional retardation at the front of a slump or slide block (Lee et al., 2007; Strachan, 2008; Van Der Merwe et al., 2011) or due to forces shoving the sediment from behind as it is forced up and over adjacent deposits (Croot, 1988; Isbell, 2010). Typically slide and slump blocks preserve internal stratification with slumps showing internal folding, typically ending in a fold nose. Formation as a slump or slide block is unlikely because no internal stratification was observed within this body and typical fold noses like those found at the front of other

slump blocks within the succession are absent. Granite boulders are also absent from all other slump or slide blocks within the study area, but are present within this facies.

Compression due to forces shoving the sediment from behind could be recognized by compressional features throughout the facies, but deformation would decrease in the direction of transport. Large pieces of excavated bedrock may also be present within the thrust sheets. There could also be older thrust sheet that are shoved up and over younger thrust sheet and truncation of the strata below within the zone of deformation (Croot, 1988; Aber et al., 1989; Isbell, 2010).

Within this facies, the sandstone thrust sheets are shoved over other thrust sheets and contain no internal folding or bedding. These bodies are underlain by the wave-rippled sandstone facies association which is interpreted to have been deposited in a shallow shelf setting with a low angle depositional slope. The association of this facies between diamictites interpreted to be the result of ice proximal glaciomarine sedimentation as mixed two component systems of iceberg rafting and settling of fines from meltwater plumes, along with the location of this facies above the interpreted wave-rippled sandstone facies, suggest that this sandstone body was the result of ice shove. Therefore, this facies is interpreted to have been formed as a glacier advanced into its deposits and shoved the sediment forward, causing thrust-faults to form (Boulton, 1986; 1990; Powell and Cooper, 2002; Isbell, 2010). This would also lead to the shearing of the diamictite directly below the facies.

5. Lithofacies Discussion

The laterally extensive sand body that contains the six measured sections for this study extends along strike from North to South along the line from A to C shown in figure 36. Several small-scale faults cut through this body. However, only a few meters of displacement occur across these faults, and the sediment body is traceable across the outcrop despite the faults. The facies that occur along the line extending from A to B are all relatively similar to one another, and the facies along the line extending from B to C are relatively similar to one another as well. These two line segments are separated by point B where the orientation of the body changes slightly with a slight increase in depositional dip. Location B also marks the point along the transect where a marked change in facies occurs.

The measured sections that fall along the line from A to B contain similar facies and are relatively similar to one another. The thin-bedded sandstone and mudstone facies, interpreted as interbedded turbidites and offshore, deep-water mudstones, is present at the base of all of the sections along the transect. The absence of wave ripples and hummocky cross-stratification indicate that these units were deposited below storm wave-base. Upward, this facies is abruptly overlain by the thick-bedded, wave-rippled facies representing deposition on a prograding shoreface above normal wave base. Trace fossils are present on some of the thin mud drapes in the lower few meters at the base of this facies. The mud becomes less frequent, and the grain size of the sandstones progressively coarsens upward from very fine to fine-grained sandstone. There are no hummocky cross-beds or current ripples present within this segment. The coarsening upward pattern along with the decrease in frequency of mud drapes in a wave-rippled

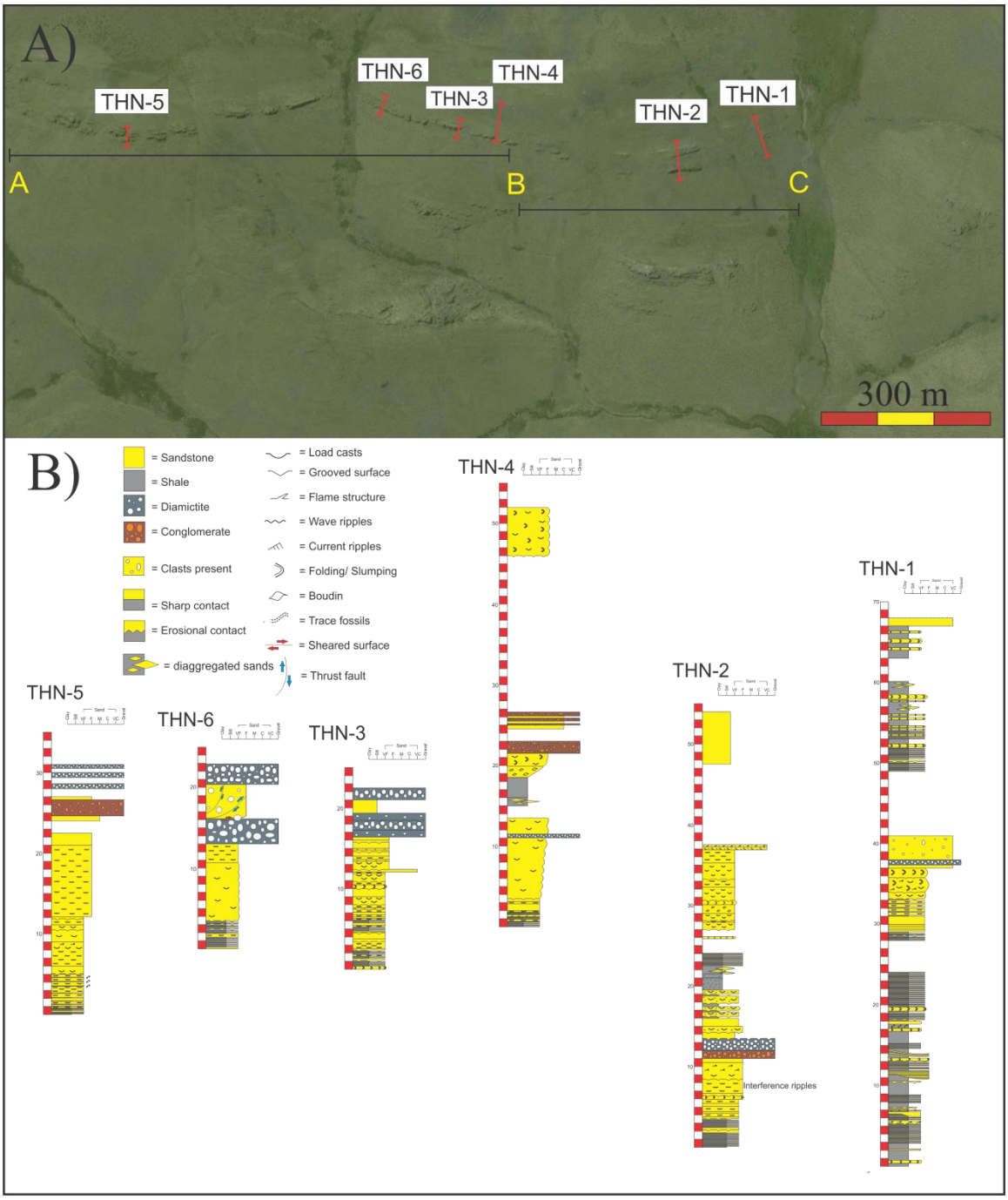

Figure 36. A) Satellite image displaying the location of the six stratigraphic columns along the lateral sand body that runs from north (A) to south (C). B) Stratigraphic columns showing the facies present in each area.

facies is typical of a shallowing upward succession within shoreface deposits (Clifton, 2006; Hampson et al., 2008; Plint, 2010; Varkarelov et al., 2012).

The large-scale loaded sandstone facies is present within the shoreface sandstones along the A to B transect. The load structures are generally underlain and overlain by the wave-rippled facies, and they also grade laterally over tens to a few hundred of meters into wave ripples. At several places within the loaded sandstone zone, wave ripples are also present. These loaded features are typical of seismites (Montenat et al., 2007; Ettensohn et al., 2011), and since they are surrounded by the thick-bedded, wave-rippled sand facies, they most likely formed from the seismic deformation of the shallowing upward shoreface succession.

Diamictite containing randomly oriented and striated clasts is interpreted to be the deposits of a two component depositional system consisting of fine-grained sediment that settled from a meltwater plume and coarse clastics introduced as ice-rafted dropstones (cf. Cowan and Powell, 1990; Cowan et al., 1999; Powell and Domack, 2002; Mugford, and Dowdeswell, 2011). This diamictite occurs at the top of the shoreface succession extending from section THN-6 to south of THN-3. Between section THN-6 and THN-3, this diamictite is sheared along its upper surface where it is overlain by the thrust-faulted, massive, boulder-bearing sandstone facies containing multiple, listric-shaped thrust faults that extend throughout the entire thickness of the unit. This sandstone does not extend across this entire segment, but it is located within section THN-6 and extents for a few hundred meters pinching out before reaching section THN-3. This facies is interpreted to be a glacially shoved deposit, possibly having originated as a grounding line fan. The underlain diamictite facies is sheared on its upper surface only where it is directly

overlain by the massive, boulder-bearing sandstone facies suggesting that these features were the result of shearing during the emplacement of the overlying blocks. This type of a deposit would be typically found near an ice margin where sediment is being shoved forward in front of an advancing ice front (Croot, 1988; Aber et al., 1989; Hart and Boulton, 1991; Lonne and Lauritsen, 1996; Bennett, 2001; Ottesen and Dowdeswell, 2006; Isbell, 2010).

The deposits from A to B are interpreted to be part of a marine shelf system. They contain facies that are typically found on the shelf such as the thick-bedded, wave-rippled facies which represents a shoreface environment (Clifton, 2006; Hampson et al., 2008; Plint, 2010; Varkarelov et al., 2012). The large-scale loaded sandstone facies that is present is also indicative of being part of the shelf system because of the wave-ripples that are present above, below, within, and lateral to this facies. The deformation is interpreted to have been at or just following deposition due to associated undeformed facies surrounding the deposits.

The normal transition in a prograding shelf succession would be deeper water deposits that were deposited below storm wave base transitioning upward into deposits that accumulated during storm events that then transition into sediment deposited above normal wave base (Clifton, 2006; Hampson et al., 2008; Plint, 2010; Varkarelov et al., 2012). Such a coarsening upward succession would be indicative of a normal regressive package that shallowed through time as the shoreface prograded basinward. The absence of sediments deposited between storm and normal wave base, characterized by hummocky cross-stratification is anomalous for such deposits. There are several possible explanations for this. They include deposition due to a forced regression where falling

relative sea level forces the facies to shift rapidly basinward resulting in an incomplete shoreface profile. Another explanation could be that sea ice was present blocking winter storm waves from reworking the bottom (Lisitzin, 2002). The presence of the deep-water deposits, interpreted to be turbidites, that were present directly below the thick-bedded, wave-rippled sandstone facies may suggest that a forced regression was at least in part responsible for the missing off-shore transition zone.

The occurrence of the thick diamictites suggest deposition from an advancing temperate glacier with deposition occurring from a two component system, which includes settling of fines from a meltwater plume and incorporation of coarse clastics from ice rafted debris (cf. Powell and Domack, 2002). This system would have included settling of fine-grained sediments from suspension and the introduction of coarse clastics as ice rafted debris. The presence of striated and bullet shaped clast suggest that icebergs rafted the clast rather than sea ice. The massive, boulder-bearing sandstone facies, which ends well before point B in the transect, suggests glacial shove from a glacier advancing across the shelf extending to near the shelf edge (cf. Aber et al., 1989; Hart and Boulton, 1991; Powell and Cooper, 2002; Isbell, 2010). Advance of a temperate glacier beyond the shelf edge is unlikely as a change in water depth would result in detachment of the glacier from its base, flotation of the ice mass, and an increase in the caving rate (Boulton, 1990)

The measured sections that fall along the transect from B to C (figure 36) contain similar facies to each other, and are interpreted to have been deposited on a submarine slope in front of the prograding shoreface deposited on the shelf and in front of a glacier that advanced to the shelf edge. The thin bedded sandstone and mudstone facies is present in all of the measured sections along this transect. Again, these deposits are

typical of turbidite deposits that form during sediment gravity flows (Hampton, 1972; Haughton et al., 2003; Amy and Talling, 2006; Talling et al., 2007; 2012). These deposits are generally found on submarine slopes and they often occur in proximity to diamictites (Haughton et al., 2003; Carto and Eyles, 2012; Talling et al., 2012). The diamictite facies that is present within this section of the outcrop is typical of debris flow deposits because they are found in proximity to interpreted slide and slump blocks and turbidites, and they consist of thin beds less than 2 meters in thickness, setting it apart from the diamictite present in the section from A to B. The upper surface of subaqueous debris flows mix with basinal waters resulting in the generation of co-linked debris flows and turbidity currents. Debris flows also transform into turbidity currents as continued mixing with basinal waters occurs during a flow (Hampton, 1972; Haughton et al., 2003; Amy and Talling, 2006; Talling et al., 2007; 2012; Carto and Eyles, 2012). The proximity of the diamictite facies to the thin-bedded sandstone and mudstone facies combined with the interpretation of deposition of the facies would indicate that the two facies were likely linked in time and space along this transect.

The deformed and undeformed sediment block facies and conglomerate and sandstone facies are also present along the sections in transect B to C. The deformed and undeformed sediment blocks are typical of slide and slumped blocks that form on unstable slopes. They may be initiated due to seismic activity, glacial advances, or overloading of sediment on a slope (Lee et al., 2007). The conglomerate and sandstone facies is interpreted to have formed from mass flows of sand and gravel. The cause of these flows could be the same as the cause of the flows for the slides and slumps. A change in slope could lead to instability and cause mass movement of sediment blocks or

sand and gravel into deeper water (Bryn et al., 2005; Lee et al., 2007; Posamentier and Walker, 2006). This results in a sandy turbidity current that leaves behind lags of pebbles and cobbles forming interbedded sands and conglomerates.

The deposits from B to C are interpreted to be part of a marine slope system. The transect south of point B contains facies such as the thin-bedded sandstone and mudstone facies, deformed and undeformed sediment blocks facies, the conglomerate and massive sands facies, and the diamictite facies. These facies all indicate that mass movement was occurring, which is typical of slope environments (Bryn et al., 2005; Posamentier and Walker, 2006; Lee et al., 2007; Strachan, 2008). These mass movement events along the slope could be triggered by a number of factors including overloading of sediment on the slope, seismic activity, or a glacial advance (Lee et al., 2007). Evidence for all three is present within the study sections.

At point B, the deposits start to change dramatically and differences can be seen in the facies that are present to the north of this point as compared to the facies that are present to the south of this point. The facies north of point B are made up of wave-ripples and massive, boulder-bearing sandstone that are interpreted to be shelf deposits. The facies south of point B contain deposits typical of turbidity currents, debris flows, and slide and slumped blocks that are interpreted to have been deposited on a marine slope. The point that separates the two sections is interpreted to be the shelf-slope break or shelf edge. This is the point on a shelf and slope system where the slope changes and sediment starts to move down slope into deeper water (figure 37) (Steel and Olsen, 2002; Steel et al., 2008). The change in slope causes the difference in the types of deposits from the shelf environment to the slope environment.

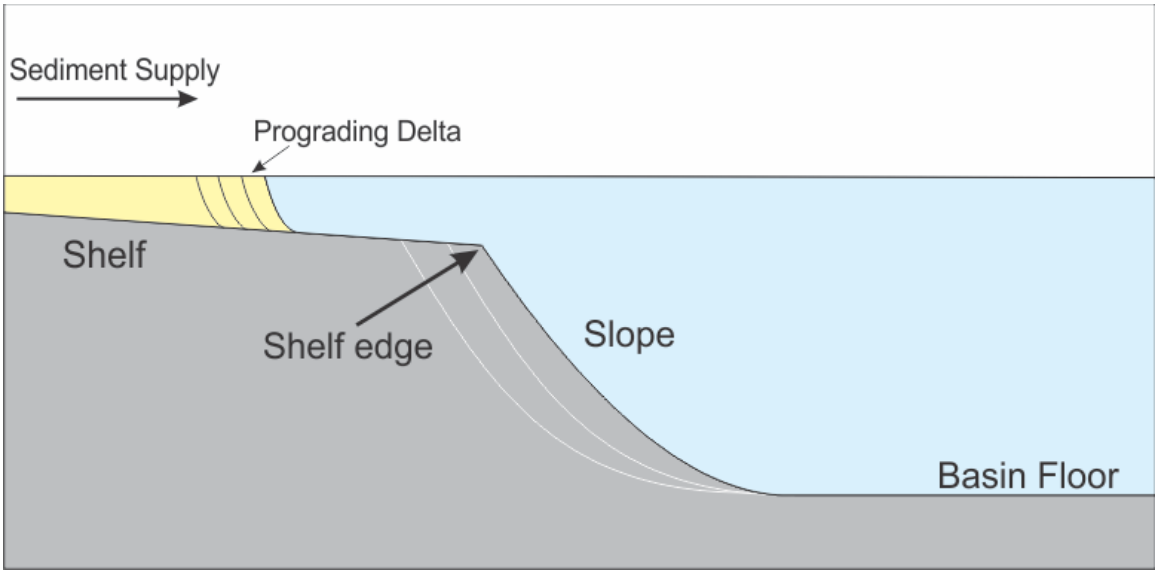

Figure 37. A shelf, shelf edge, slope, and basin floor environment. The angle of the slope and the shelf are exaggerated.

The laterally extensive sand body that runs from north to south is interpreted to be an outer shelf, shelf-slope break, and slope environment (figure 38). The deposits transition from shallower water deposits in the north to deeper water deposits heading south along the sand body. The presence of deposits formed from mass movement along a slope indicate that the shelf-slope break would be located near point B where there is a change in slope, and the cause of the mass movement could be from either seismic activity, a glacial advance, overloading of sediment, or all three.

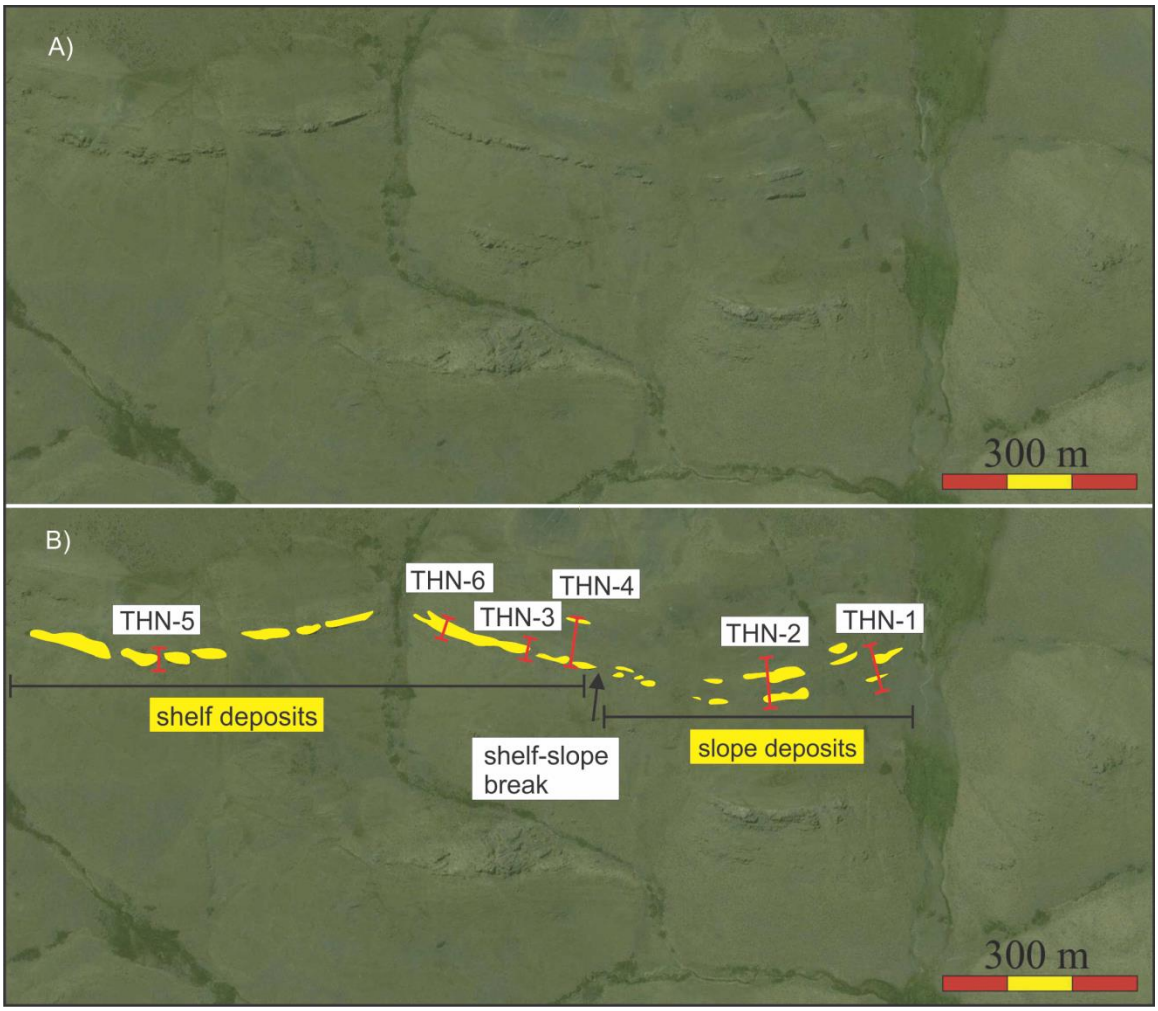

Figure 38. A) A satellite image of the lateral sand body extending from north to south. B) Sand bodies are highlighted in yellow. Shelf deposits are present in the northern section and slope deposits are present in the section to the south.

6. **Sequence Stratigraphy**

The Tepuel-Genoa basin contains deposits from a glacially influenced outer shelf, basin slope, and basin floor setting under high subsidence rates which forms a 5,000+ meter thick succession of glaciomarine and glacially influenced deposits (Lopez Gamundi et al., 1994; Taboada, 2010; Isbell et al., 2013b). These deposits consist of stacked successions of thick (100's of meters), fossil and dropstone-bearing, marine shales capped by sandstones and diamictites that measure 10's of meters in thickness.

The coarse clastic interval investigated represents clinoform deposits composed of a shallow-water shelf succession of shoreface and ice proximal glaciomarine deposits that transitions laterally in to a slope succession composed of mass movement (slide and slump blocks), debris flow, and turbidite deposits. Directly below the shoreface deposit is a thick succession of mudstone that contains marine fossils of the *Lanipustula* Biozone(Pagani and Taboada, 2010; Pauls, 2014). This succession of mudstone also contains scattered large sand bodies interpreted as slide and slump blocks (Pauls, 2014). The study section is overlain by shale that contains slump blocks and an absence of wave indicators suggesting deposition well-below wave base. Although not investigated in the field, satellite images reveal two additional shale to sandstone successions. Ridge forming sandstones at the top of these successions are of equivalent thickness to the studied sandstones, and contain foreset beds that display an apparent depositional dip towards the south. The sandstones can be traced southward up to 1.5 km where they end in a dipping zone of discontinuous blocks of sandstones similar to the shelf-slope clinoform studied here (figure 39). Therefore, these clinoforms are also interpreted as prograding shelf deposits.

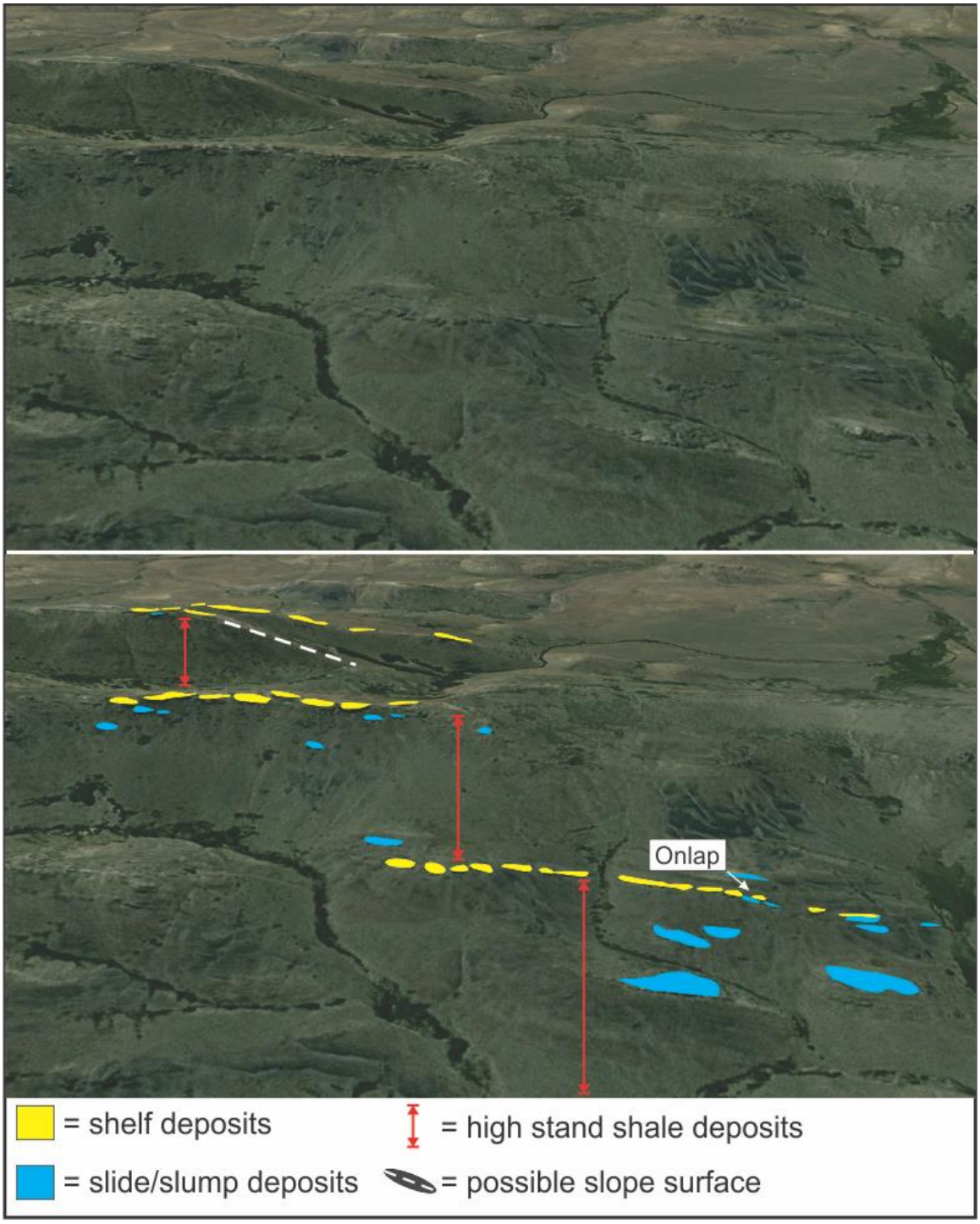

Figure 39. Google Earth image of part of the Pampa de Tepuel Formation. There are thick successions of shale containing slide/slumped blocks that are capped by sandstone shoreface deposits.

Within the study section, shoreface deposits rest directly on offshore shales. Within this coarsening upward succession, deposits of the offshore transition zone, which are those units deposited between normal and storm wave base typified by interbedded hummocky sandstones and shales, are absent. This pattern is not representative of units deposited under conditions of a normal regression or progradation of shelf deposits under static or rising relative sea level (eustatic sea level + subsidence). Under a normal regression, sediments transition upward from offshore mudrocks to interstratified sandstone and mudrock of the offshore transition zone and into coarse-clastics shoreface deposits. The absence of the offshore transition zone in the study section is more typical of a forced regression (Plint, 1988; Clifton, 2006; Plint, 2010). In a forced regression, the rapid basinward shift of environments during a relative fall in sea level often results in missing environments within a shoreface succession.

Further evidence for a forced regression occurs to the south of the interpreted shelf slope break (see previous chapter). In this area, onlap of rippled shoreface sandstones occurs (section THN-2) onto the dipping slope clinoform (Figures 40, 41, and 42). Such onlap can only occur if relative sea level fell below the shelf-slope break. The slump blocks that are above the measured sections within the shale may have formed during a transgression. As sea level rises, sliding and slumping can occur on the slope as the active coarse-grained sedimentation steps towards the basin margin. However, the slump deposits could be part of the overlying coarsening-upward succession where the slump may have slid down the slope to the basin floor as part of the progradation of the overlying shelf during the next fall in relative sea level. Slides and slumps can travel

long distances, so they could be far traveled down the slope where further sedimentation completely buried the slump block in a thick mudrock succession.

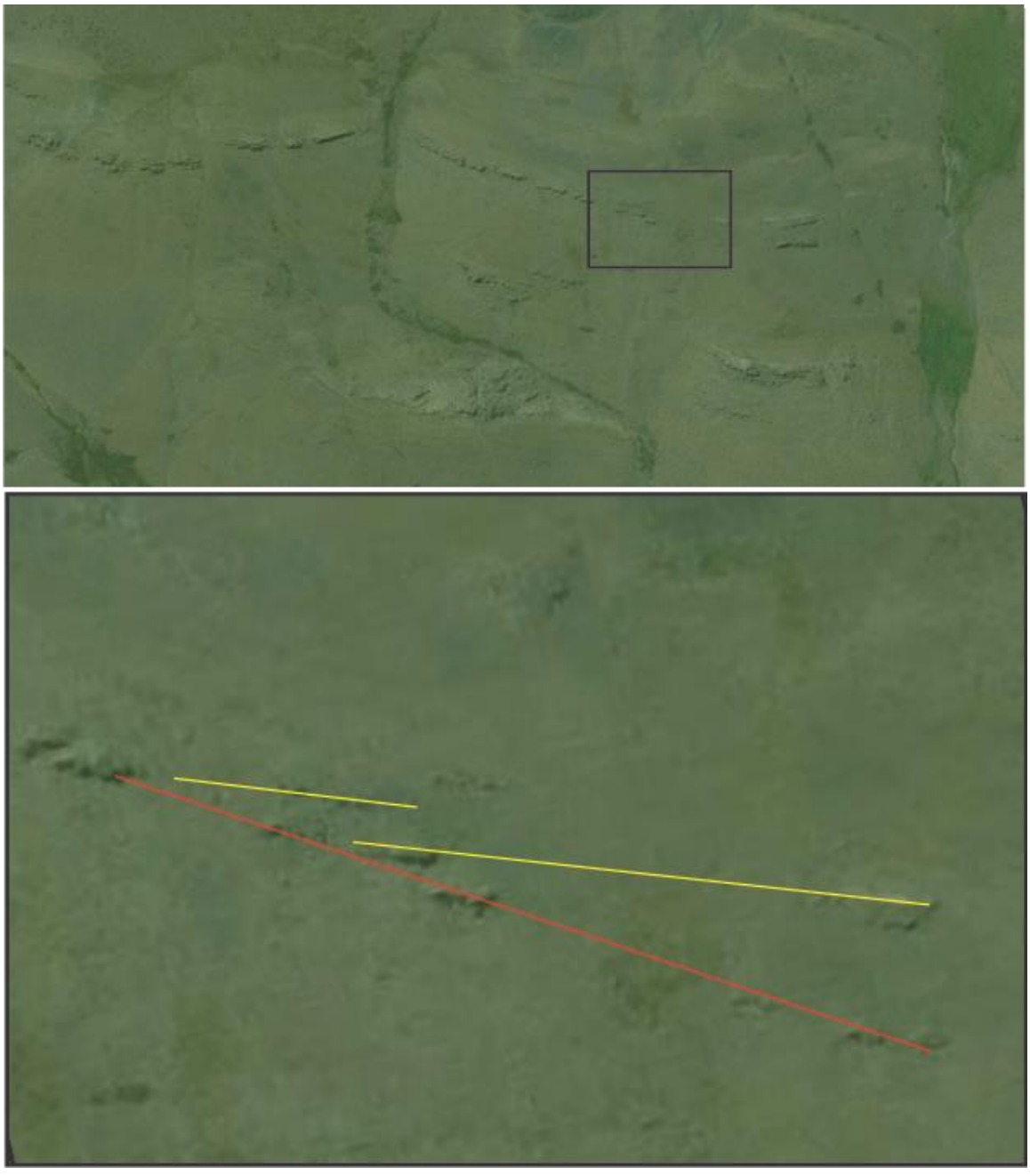

Figure 40. Satellite image that is showing onlap. The slope is shown in red and the bedding that is onlapping is shown in yellow.

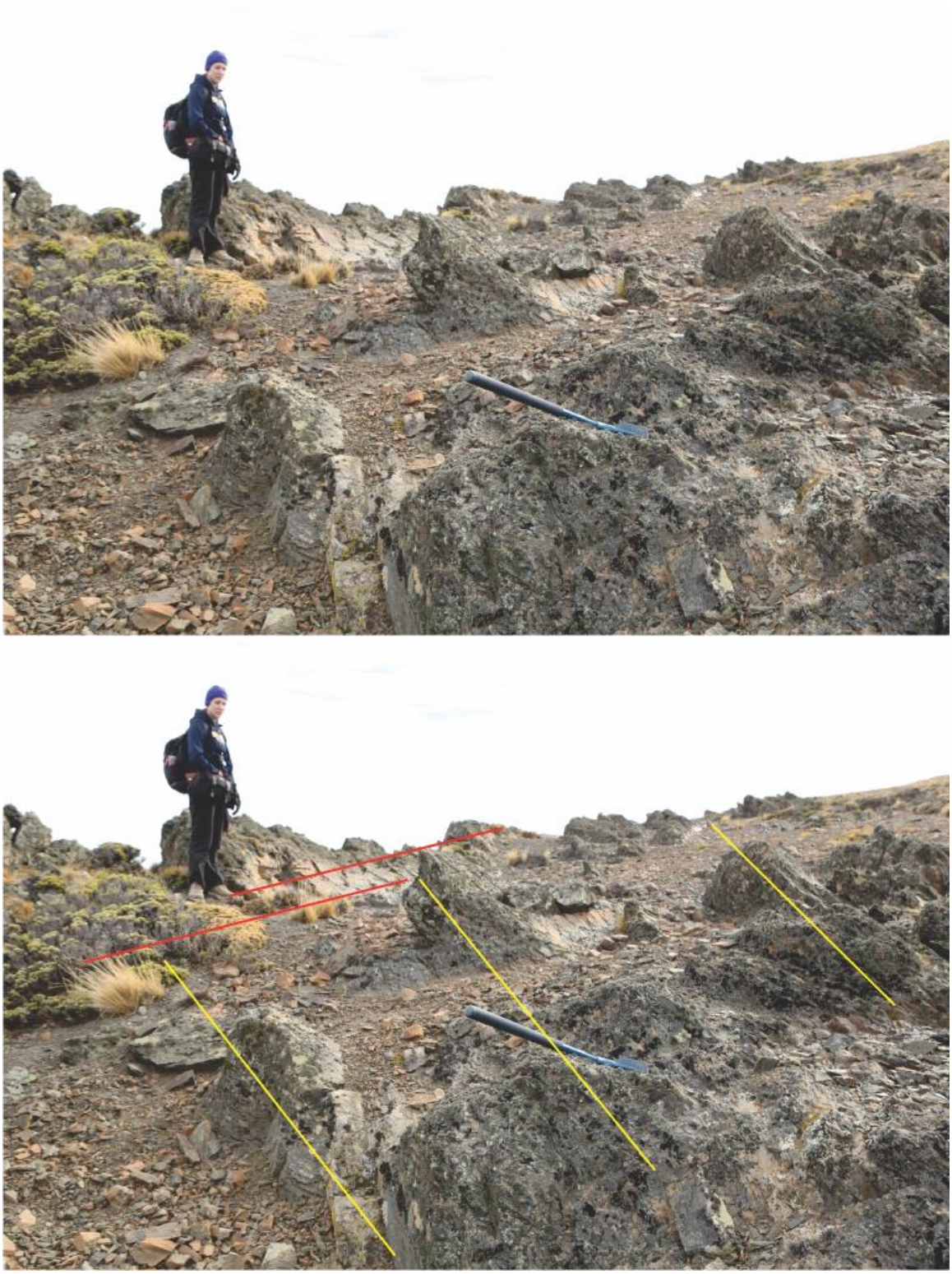

Figure 41. Photo showing onlap. The bedding of the slope is shown in red and the bedding that is onlapping is shown in yellow. Person for scale.

Figure 42. Photo showing onlap. The red line represents the slope and the yellow lines represent the bedding that is onlapping. People for scale.

Images from Google Earth and previous field work suggests that this pattern repeats throughout deposition of the Pampa de Tepuel deposition, both at Tepuel Hill further up in section and elsewhere in the basin. Above the black shales there appears to be another shelf and slope sand body. Smaller blocks of sand occur beneath this sand

body, which are here interpreted as slump blocks contained within the mudrock facies. Near the top of the Tepuel Hill section, a similar third succession also occurs (figure 43). Further work in the area could be done to determine if these sand bodies are the result of a forced regression as well and to further develop the sequence stratigraphy of the basin.

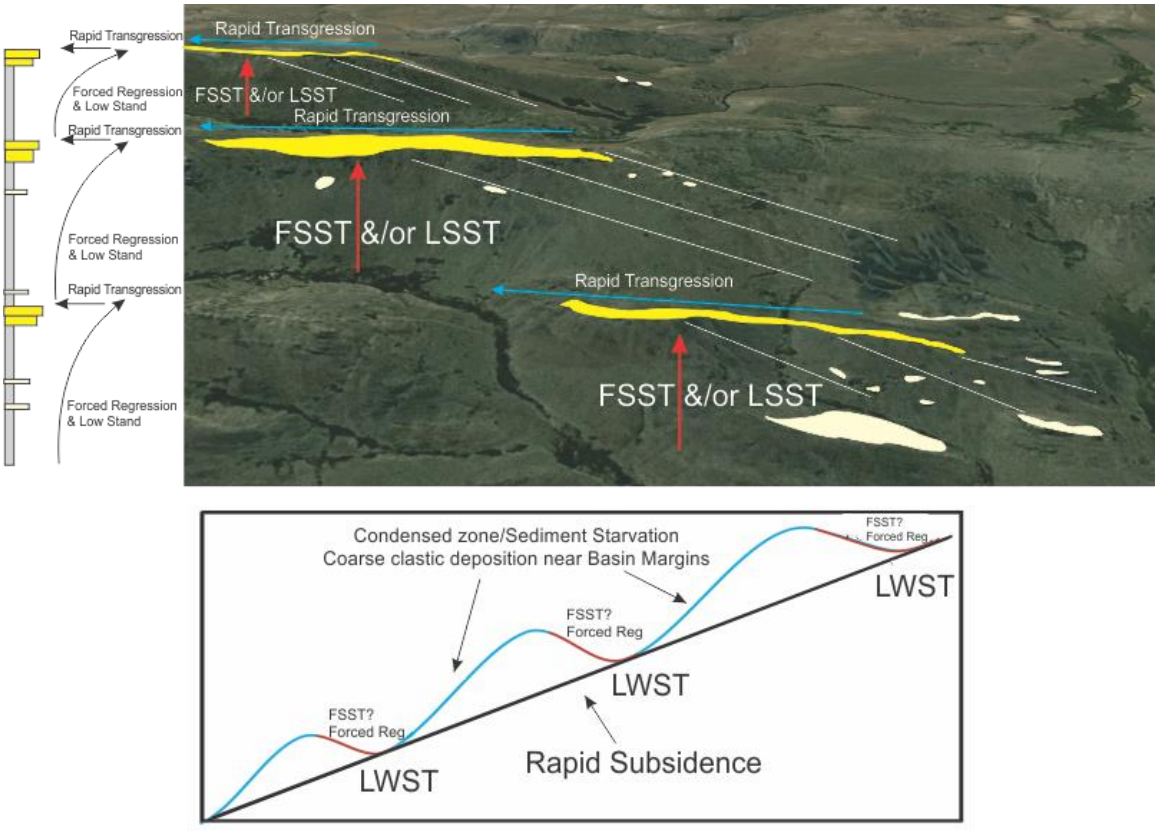

Figure 43. The image shows the transgressive surfaces and the falling stage systems tract. The sand bodies highlighted in yellow are the shelf and upper slope deposits, and the sand bodies highlighted in tan represent slide and slump blocks. The generalized strat column shows predictions that the upper two sand bodies may represent forced regressions. The generalized accommodation curve demonstrates what is occurring in this location of the basin.

The majority of the sediment within the basin would have been deposited during a falling stage systems tract. As sea level begins to drop, sediment can be carried out deeper into the basin. The thick mud would have been deposited at this time when sea

level was falling and the mud was carried out further into the basin. During transgression and early high stand stages of a relative sea level cycle, clastics are trapped on the shelf and do not make it to the shelf edge. The slide and slump blocks could also have been deposited during a forced regression when enhanced sedimentation at the shelf edge results in over steepening of the depositional slope and failure causes a slide to occur. The shore face deposits would have made it out into the basin during a low stand when a forced regression occurred. This would have left coarser material deposited directly on top of mud and deeper water deposits.

A rapid transgression occurred after the deposition of the sand blocks leaving the area sediment starved as indicated by an absence of shallow water indicators in the overlying shale. At this time, deposition occurred at the basin margins, but no coarse clastics were making it out to the deeper parts of the basin. Some of the mud above the sand bodies may have been deposited during the initial stages of the transgression, but the majority of the thick mudrock succession would have been deposited when the sea level began to drop and the clastic material began to build out into the basin again. The slide and slump blocks that are present within the mud directly above the sand bodies may have been deposited when sea level began to rise during the initial stage of the transgression. The rise in sea level could have caused instability which lead to sliding and slumping.

Evidence for glaciation was present within the studied sections as indicated by the thick diamictite deposit, a few bulleted and striated clasts, and the thrust-faulted, boulder-bearing sandstone body that is interpreted to have been deposited when a glacier shoved the sediment in front of it forward. These glacial deposits were present stratigraphically

above the shoreface deposits suggesting that as sea level was falling, a glacier was advancing to the shelf edge. The outcrop that was studied is in the *Lanipustula* Biozone making it roughly Serpukovian to Early Muscovian in age. A glacial advance is seen in the Rio Blanco Basin and the Paganzo Basin in the late Serpukhovian to the early Bashkirian and in the Paganzo Basin in the late Bashkirian (Gulbranson et al., 2010). This may suggest that the eustatic drop in sea level could have been caused by the advancing of glaciers in Gondwana. Without a better age constrain on the outcrop within the Tepuel Basin, it is difficult to correlate this glacial advance to other advances seen in Gondwana.

7. Conclusion

The Late Paleozoic Ice Age lasted from the Carboniferous into the Permian, and part of the record of the ice age is recorded within the Tepuel-Genoa Basin. The lateral sand body, and its associated facies that were studied within the basin, show evidence that sedimentary rocks in the study area were deposited on a basin shelf, shelf edge, and basin slope environment. Thick shoreface deposits containing mainly wave-rippled, fine-grained sandstone with some interference ripples are evidence that the deposits from A-B were shelf deposits. The deposits from B-C were mainly deposits formed through slumping and sliding and gravity flows giving evidence of an upper slope environment. The mudrock and the lateral sand body are part of a forced regression that caused the mud and eventually the sand to migrated basinward over slope deposits as sea level dropped. The lack of a transition zone between the deep water turbidite deposits and the wave-rippled sandstones is evidence that sea level dropped rapidly and the storm wave-base deposits never formed. Above the study section is more mudrock indicating that a rapid transgression would have occurred, and the coarser clastic deposition would have moved closer to the basin margin. To get the thick succession of mudrock, another forced regression would have occurred in order to deposit the sediment out to this point in the basin. The sliding and slumping on the slope could have occurred because of the seismic activity, a glacial advance, a change in sea level, or overloading of sediment on the slope.

Evidence for a glacial advance was present within the study section. This was seen in section THN-6 which contained relatively thick diamictite deposits that were topped by thrust-faulted, massive, boulder-bearing sandstone containing listric-shaped

faults. These deposits were interpreted to have formed from grounding line processes which is evidence for a glacier being present in the area and advancing to the shelf edge, shoving the grounding line sands forward. This glacial advance may have contributed to the relative fall in sea level that is seen in this portion of the basin if it were part of a large-scale climate cycle influencing other glaciers across Gondwana, but without a better age control on the basin, it is difficult to correlate the timing of known glacial advances with the advance seen at this outcrop.

References

Aber, J.S., Croot, D.G., and Fenton, M.M., 1989, Glaciotectonic landforms and structures: Dordrecht, Kluwer Academic Publisher, 200 p.

Allen, J.R.L., 1984, Developments in sedimentology: New York, Elsevier Science Publishers, 661 p.

Amy, L. and Talling, P. J., 2006, Anatomy of turbidite and debrite sandstones based on long distance (120 · 35 km) bed correlation, Marnoso-arenacea Formation, Northern Apennines, Italy: Sedimentology, v. 53, p. 161-212.

Andreis, R. R., Archangelsky, S., Gonzalez, C. R., Lopez Gamundi, O., Sabattini, N., Acenolaza, F. G., Azcuy, C. L., Cortinas, J., Cuerda, A., and Cuneo, R., 1987, Cuenca Tepuel-Genoa, in Archangelsky, S., ed., El Sistema Carbonifero en la República Argentina, Academia Nacional De Ciencias de Cordoba, p. 169-196.

Bennett, M. R., 2001, The morphology, structural evolution and significance of push moraines: Earth-Science Reviews, v. 53, p. 197-236.

Bezerra, F. H. R., da Fonseca, V. P., and Lima Filho, F. P., 2001, Seismites; origin, criteria for identification and examples from the quaternary record of northeastern brazil: Pesquisas Em Geociencias, v. 28, p. 205-212.

Birgenheier, L. P., Fielding, C. R., Rygel, M. C., Tracy D. Frank, and Roberts, J., 2009, Evidence for dynamic climate change on sub-106-year scales from the late Paleozoic Glacial record, Tamworth Belt, New South Wales, Australia: Journal of Sedimentary Research, v. 79, p. 56-82.

Blakey, R.C., 2008, Gondwana paleogeography from assembly to breakup- a 500 m.y. odyssey, in Fielding, C.R., Frank, T.D., Isbell, J.L., eds., Resolving the Late Paleozoic Ice Age in Time and Space: Geological Society of America Special Papers 441, p. 1-28.

Boulton, G.S., 1986, Push-moraines and glacier-contact fans in marine and terrestrial environments: Sedimentology, v. 33, p. 677-698.

Boulton, G.S., 1990, Sedimentary and sea level changes during glacial cycles and their control on glacimarine facies architecture, in Dowdeswell, J.A., and Scourse, J.D., eds., Glacimarine environments: processes and sediment, Volume Special Publication 53, Geological Society, p. 15-52.

Bryn, P., Kjell, B., Forsberg, C.F., Solheim, A., Kvalstad, T.J., 2005, Explaining the Storrega Slide: Marine & Petroleum Geology, v. 22, p. 11-19.

Buggisch, W., Wang, X., Alekseev, A.S., and Joachimski, M.M., 2011, Carboniferous-Permian carbon isotope stratigraphy of successions from China (Yangtze platform), USA (Kansas) and Russia (Moscow Basin and Urals): Palaeogeography, Palaeoclimatology, and Palaeoecology 301, p. 18-38.

Callot, P., Odonne, F., Debroas, E., Maillard, A., Dhont, D., Basile, C., and Hoareau, G., 2009, Three-dimensional architecture of submarine slide surfaces and associated soft-sediment deformation in the Lutetian Sobrarbe deltaic complex (Ainsa, Spanish Pyrenees): Sedimentology, v. 56, p. 1226-1249.

Caputo, M.V., Melo, J.H.G. de, Streel, M., and Isbell, J.L., 2008, Late Devonian and Early Carboniferous glacial records of South America, *in* Fielding, C.R., Frank, T.D., and Isbell, J.L., eds., Resolving the Late Paleozoic Ice Age in Time and Space: Geological Society of America Special Paper 441, p. 161–173.

Carto, S.L., and Eyles, N., 2012, Identifying glacial influences on sedimentation in tectonically-active, mass flow dominated arc basins with reference to the Neoproterozoic Gaskiers glaciation (c. 580 Ma) of the Avalonian-Cadomian orogenic belt: Sedimentary Geology, v. 261-262, p. 1-14.

Clifton, H.E., 2006, A reexamination of facies models for clastic shorelines: Special Publication - Society for Sedimentary Geology, v. 84, p. 293-337.

Collinson, J., Mountney, N., and Thompson, D., 2006, Sedimentary structures: England, Terra Publishing, 3rd ed., 292 p.

Cowan, E.A. and Powell, R.D., 1990, Suspended sediment transport and deposition of cyclically interlaminated sediment in a temperate glacial fjord, Alaska, U.S.A., in Dowdeswell, J.A. and Scourse, J.D., eds., Glacimarine Environments: Processes and Sediments: Geological Society Special Publication, no. 53, p. 75-89.

Cowan, E. A., Seramur, K. C., Cai, J., and Powell, R.D., 1999, Clyclic sedimentation produced by fluctuations in meltwater discharge, tides and marine productivity in an Alaskan fjord: Sedimentology, v. 46, p. 1109-1126.

Croot, D. G., 1988, Morphological, structural and mechanical analysis of neoglacial ice-pushed ridges in Iceland, in Croot, D. G., ed., Glaciotectonics: forms and processes: Rotterdam, A.A. Balkema, p. 33-47.

Dowdeswell, J.A., Whittington, R.J., and Marienfeld, P., 1994, The origin of massive diamicton facies by iceberg rafting and scouring, Scoresby Sund, East Greenland: Sedimentology, v. 41, p. 21-35.

Eros, J.M., Montanez, I.P., Osleger, D.A., Davydov, V.I., Nemyrovska, T.I., Poletaev, V.I., and Zhykalyak, M.V., 2012, Sequence stratigraphy and onlap history of the Donets Basin, Ukraine: Insight into Carboniferous icehouse dynamics: Palaeogeography, Palaeoclimatology, Palaeoecology, v. 313-314, p. 1-25.

Ettensohn, F. R., Zhang, C., Gao, L., and Lierman, R. T., 2011, Soft-sediment deformation in epicontinental carbonates as evidence of paleoseismicity with evidence for a possible new seismogenic indicator: Accordion folds: Sedimentary Geology, v. 235, p. 222-233.

Eyles, C.H., Eyles, N., and Miall, A. D., 1985, Models of glaciomarine sedimentation and their application to the interpretation of ancient glacial sequences: Palaeogeography, Palaeoclimatology, Palaeoecology, v. 51, no. 1-4, p. 15-84.

Eyles, N., Eyles, C. H., and Miall, A.D., 1983, Lithofacies types and vertical profile models; an alternative approach to the description and environmental interpretation of glacial diamict and diamictite sequences: Sedimentology, v. 30, p. 393-410.

Eyles, N., Franca, A. B., Gonzalez Bonorino, G., Eyles, C. H., and Lopez Paulsen, O., 1995, Hydrocarbon-bearing Late Paleozoic glaciated basins of southern and central South America, in Tankard, A. J., Suarez, R., and Welsink, H. J., Petroleum basins of South America: AAPG Memoir 62, p. 165-183.

Fielding, C. R., Frank, T. D., Birgenheier, L. P., Rygel, M. C., Jones, A. T., and Roberts, J., 2008a, Stratigraphic imprint of the late Palaeozoic ice age in eastern Australia: a record of alternating glacial and nonglacial climate regime: Journal of the Geological Society, London, v. 165, p. 129-140.

Fielding, C. R., Frank, T. D., Birgenheier, L. P., Rygel, M. C., Jones, A. T., and Roberts, J., 2008b, Stratigraphic record and facies associations of the late Paleozoic ice age in eastern Australia (New South Wales and Queensland), in Fielding, C. R., Frank, T., and Isbell, J. L., eds., Resolving the Late Paleozoic Ice Age in Time and Space: Boulder, CO, Geological Society of America Special Paper 441, p. 41-57.

Fielding, C. R., Frank, T. D., and Isbell, J. L., 2008c, The late Paleozoic ice age—A review of current understanding and synthesis of global climate patterns: Geological Society of America Special Papers, v. 441, p. 343-354.

Freytes, E., 1971, [Informe geológico preliminary sobre la Sierra de Tepuel (Deptos. Languiñeo y Tehuelches, prov. de Chubut). Informe YPF. Inédito.]

Gilbert, R., 1990, Rafting in glacimarine environments, in Dowdeswell, J. A., and Scourse, J. D., eds., Glacimarine environments: processes and sediments: Geological Society Special Publications, v. 53, p. 105-120.

González Bonorino, G., Ratine, G., Vega, V., Guerin, D., 1988. Ambientes de plataforma neritica dominada por tormentas en la seccion glacignica del Grupo Tepuel, Chubut Rev. Asociacion Geologica Argentina 43, 239-252.

González-Bonorino, G., 1992, Carboniferous glaciation in Gondwana. Evidence for grounded marine ice and continental glaciation in southwestern Argentina: Palaeogeography, Palaeoclimatology, Palaeoecology, v. 91, p. 363-375.

González-Bonorino, G. and Eyles, N., 1995, Inverse relation between ice extent and the late Paleozoic glacial record of Gondwana: Geology, v. 23, p. 1015-1018.

González, C.R., Taboada, A.C., Díaz Saravia, P.G., Andres, M.A., 1995. El Carbónico del sector noroccidental de la Provincia del Chubut. Revista de la Asociacion Geologica Argentina 50, 40-46.

González, C.R., and Díaz Saravia, P., 2010, Bimodal character of the Late Paleozoic glaciations in Argentina and bipolarity of climatic changes: Palaeogeography, Palaeoclimatology, Palaeoecology, v. 298, 101-111.

Greb, S. F., Ettensohn, F. R., and Obermeier, S. F., 2002, Developing a classification scheme for seismites: Abstracts with Programs - Geological Society of America, v. 34, p. 102.

Gulbranson, E. L., Montanez, I. P., Schmitz, M. D., Limarino, C. O., Isbell, J. L., Marenssi, S. A., and Crowley, J. L., 2010, High-precision U-Pb calibration of Carboniferous glaciation and climate history, Paganzo Group, NW Argentina: Geological Society of America Bulletin, v. 122, p. 1480-1498.

Hambrey, M.J., Ehrmann, W.U., and Larsen, B., 1991, Cenozoic glacial record of the Prydz Bay continental shelf, East Antarctica, in Barron, J. and Larsen, B., eds., Proc. Ocean Drilling Program Scientific Results, v. 119, p. 77-131.

Hampson, G.J., Rodriguez, A.B., Storms, J.E.A., Johnson, H.D., and Meyer, C.T., 2008, Geomorphology and high-resolution stratigraphy of progradational wave-dominated shoreline deposits: Impact on reservoir-scale facies architecture: SEPM Special Publication, no. 90, p. 117-142.

Hampton, M. A., 1972, The role of subaqueous debris flow in generating turbidity currents: Journal of Sedimentary Petrology, v. 42, no. 4, p. 775-793.

Hart, J.K., and Boulton, G.S., 1991, The interrelation of glaciotectonic and glaciodepositional processes within the glacial environment: Quaternary Science Reviews, v. 10, p. 335–350.

Haughton, P. D. W., Barker, S. P., and McCaffrey, W. D., 2003, 'Linked' debrites in sand-rich turbidite systems-origin and significance: Sedimentology, v. 50, p. 459-482.

Haughton, P.D.W., Davis, C., McCaffrey, W. and Barker, S., 2009, Hybrid sediment gravity flow deposits – classification, origin and significance: Marine Petroleum Geology, v. 26, p. 1900–1918.

Heckel, P.H., 1994, Evaluation of evidence for glacio-eustatic control over marine Pennsylvanian cyclothems in North America and consideration of possible tectonic effects, *in* Dennison, J. M., and Ettensohn, F. R., eds., Tectonic and eustatic controls on sedimentary cycles, Volume Concepts in Sedimentology and Paleontology Volume 4: Tulsa, SEPM (Society of Sedimentary Geology), p. 65-87.

Henry, L. C., Isbell, J. L., and Limarino, C. O., 2008, Carboniferous glacigenic deposits of the proto-Precordillera of west-central Argentina, in Fielding, C. R., Frank, T. D., and Isbell, J. L., eds., Resolving the Late Paleozoic Ice Age in Time and Space:: Boulder, CO, Geological Society of America Special Publication., p. 131-142.

Henry, L. C., Isbell, J. L., Limarino, C. O., McHenry, L. J., and Fraiser, M. L., 2010, Mid-Carboniferous deglaciation of the Protoprecordillera, Argentina recorded in the Agua de Jaguel palaeovalley: Palaeogeography Palaeoclimatology Palaeoecology, v. 298, no. 1-2, p. 112-129.

Henry, L. C., Isbell, J. L., Fielding, C. R., Domack, E. W., Frank, T. D., and Fraiser, M. L., 2012, Proglacial deposition and deformation in the Upper Carboniferous to Lower Permian Wynyard Formation, Tasmania: A process analysis: Palaeogeography, Palaeoclimatology, Palaeoecology, v. 315-316, p. 142-157.

Isbell, J. L., Miller, M. F., Babcock, L.E., and Hasiotis, S.T., 2001, Ice-marginal environment and ecosystem prior to initial advance of the late Palaeozoic ice sheet in the Mount Butters area of the central Transantarctic Mountains, Antarctica: Sedimentology, v. 48, p. 953-970.

Isbell, J. L., Miller, M. F., Wolfe, K. L., and Lenaker, P. A., 2003, Timing of late Paleozoic glaciation in Gondwana: was glaciation responsible for the development of northern hemisphere cyclothems?, in Chan, M. A., and Archer, A. W., eds. Extreme depositional environments: mega end members in geologic time, Volume 370: Boulder, Colorado, Geological Society of America Special Paper, p. 5-24.

Isbell, J. L., Koch, Z. J., Szablewski, G. M., and Lenaker, P. A., 2008a, Permian glacigenic deposits in the Transantarctic Mountains, Antarctica, in Fielding, C. R., Frank, T. D., and Isbell, J. L., eds., Resolving the Late Paleozoic Ice Age in Time and Space:: Boulder, CO, Geological Society of America Special Publication., p. 59-70.

Isbell, J. L., Cole, D. I., and Catuneanu, O., 2008b, Carboniferous-Permian glaciation in the main Karoo Basin, South Africa: stratigraphy, depositional controls, and glacial dynamics, in Fielding, C. R., Frank, T. D., and Isbell, J. L., eds., Resolving the Late Paleozoic Ice Age in Time and Space:: Boulder, CO, Geological Society of America Special Paper 441., p. 71-82.

Isbell, J.L., 2010, Environmental and paleogeographic implications of glaciotectonic deformation of glaciomarine deposits within Permian strata of the Metschel Tillite, southern Victoria Land, Antarctica: The Geological Society of America Special Paper 468, p. 81-100.

Isbell, J.L., Henry, L.C., Limarino, C.O., Koch, Z.J., Ciccioli, P.L., and Fraiser, M.L., 2011, The equilibrium line altitude as a control on Godwana Glaciation during the late Paleozoic Ice Age, in Hakansson, E., and Trotter, J., eds., Programme & Abstracts: The XVII International Congress on the Carboniferous and Permian, Perth 3-8, July 2011, Volume Record 2011/20, Geological Survey of Western Australia, p. 74.

Isbell, J. L., Henry, L. C., Gulbranson, E. L., Limarino, C. O., Fraiser, M. L., Koch, Z. J., Ciccioli, P. L., and Dineen, A. A., 2012, Glacial paradoxes during the late Paleozoic ice age: Evaluating the equilibrium line altitude as a control on glaciation: Gondwana Research, v. 22, p. 1-19.

Isbell, J.L., Taboada, A.C., Gulbranson, E.L., Pagani, M.A., Pauls, K.N., Limarino, C.O., Ciccioli, P.L., Fraiser, M.L., 2013a, Carboniferous and Permian glacigenic and non-glacial strata of the Tepuel-Genoa Basin, Patagonia, Argentina: A near-continuous, deep-water record of South Polar Gondwana during the late Paleozoic Ice Age: Geological Society of America Abstracts with Programs, v. 45, no. 7.

Isbell, J. L., Henry, L. C., Reid, C. M., and Fraiser, M. L., 2013b, Sedimentology and palaeoecology of lonestone-bearing mixed clastic rocks and cold-water carbonates of the Lower Permian Basal Beds at Fossil Cliffs, Maria Island, Tasmania (Austrailia): Insight into the initial decline of the late Palaeozoic ice age, in Gasiewicz, A. and Slowakiewicz, M., eds., Palaeozoic climate cycles: Their evolutionary and sedimentological impact: Geological Society of London, Special Publication 376.

Lee, H. J., Locat, J., Desgagnes, P., Parsons, J. D., McAdoo, B. G., Orange, D. L., Puig,

P., Wong, F. L., Dartnell, P., and Boulanger, E., 2007, Submarine mass movements on continental margins: Special Publication of the International Association of Sedimentologists, v. 37, p. 213-274.

Limarino, C. O. and Spalletti, L. A., 2006, Paleogeography of the upper Paleozoic basins of southern South America: An overview: Journal of South American Earth Sciences, v. 22, p. 134-155.

Lindsay, J.F., 1970, Depositional environment of Paleozoic glacial rocks in the central Transantarctic Mountains: Geological Society of America Bulletin, v. 81, p. 1149–1172.

Lisitzin, A.P., 2002, Sea-ice and iceberg sedimentation in the ocean: Springer-Verlag Berlin Heidelberg, 563 p.

Lonne, I., and Lauritsen, T., 1996, The architecture of a modern push-moraine at Svalbard as inferred from ground-penetrating radar measurements: Arctic and Alpine Research, v. 28, p. 488-495.

López-Gamundí, O. R. and Limarino, C.O., 1984, Facies de abanico submarine en el Grupo Tepuel (Paleozoico Superior) Provincia del Chubut: Asociacion Geologica Argentina, v. 3-4, p. 251-261.

López-Gamundí, O. R., Espejo, I. S., Conaghan, P. J., and Powell, C. McA., 1994, Southern South America, in Veevers, J. J., and Powell, C. McA., eds., Permian-Triassic Pangean basins and foldbelts along the Panthalassan Margin of Gondwanaland: Boulder, CO, Geological Society of America Memoir 184, p. 281-329.

López-Gamundí, O. R., 1997, Glacial-postglacial transition in the Late Paleozoic basins of southern South America, in Martini, I. P., ed., Late glacial and postglacial environmental changes: Quaternary, Carboniferous-Permian, and Proterozoic: Oxford, U.K., Oxford University Press, p. 147-168.

Montañez, I. P., and Poulsen, C. J., 2013, The late Paleozoic ice age: an evolving paradigm: Annual Review of Earth & Planetary Sciences, v. 41, no. 24, p. 1-28.

Montenat, C., Barrier, P., Ott d'Estevou, P., and Hibsch, C., 2007, Seismites: An attempt at critical analysis and classification: Sedimentary Geology, v. 196, p. 5-30.

Mory, A. J., Redfern, J., and Martin, J. R., 2008, A review of Permian-Carboniferous deposits in Western Australia, in Fielding, C. R., Frank, T. D., and Isbell, J. L., eds., Resolving the Late Paleozoic Ice Age in Time and Space:: Boulder, CO, Geological Society of America Special Paper 441., p. 71-82.

Mugford, R. I., and Dowdeswell, J. A., 2011, Modeling glacial meltwater plume

dynamics and sedimentation in high-latitude fjords: Journal of Geophysical Research, v. 116.

Mulder, T., and Alexander, J., 2001, The physical character of subaqueous sedimentary density flows and their deposits: Sedimentology, v. 48, no. 2, p. 269-299.

Ottesen, D., and Dowdeswell, J. A., 2006, Assemblages of submarine landforms produced by tidewater glaciers in Svalbard: J. Geophys. Res., v. 111, no. F1, p. F01016.

Pagani, M.A. and Taboada, A.C., 2010. The marine upper Paleozoic in Patagonia (Tepuel Genoa Basin, Chubut Province, Argentina): 85 years of work and future prospects. Palaeogeography, Palaeoclimatology, Palaeoecology 298, 130-151.

Pauls, K.N., 2014, Sedimentology and Paleoecology of fossil-bearing, high-latitude marine and glacially influenced deposits in the Tepuel Basin, Patagonia, Argentina [M.S. Thesis]: Milwaukee, University of Wisconsin, 157 p.

Plint, A.G., 1998, Sharp-based shoreface sequences and "offshore bars" in the Cardium Formation of Alberta: their relationship to relative changes in sea level, in Wilgus, C.K., Hastings, B.S., Kendall, C.G.St.G., Posamentier, H.W., Ross, C.A., and Van Wagoner, J.C., eds., Sea Level Changes: An Integrated Approach: SEPM, Special Publication 42, P. 357-370.

Plint, A.G., 2010, Wave- and storm-dominated shoreline and shallow-marine systems, in James, N. P. and Dalrymple, R.W., eds., Facies Models 4: Canadian Sedimentolgy, p. 167-199.

Posamentier, H.W., and Walker, R.G., 2006, Deep-water turbidites and submarine fans, in Posamentier, H. W., and Walker, R. G., eds., Facies models revisited: Tulsa, SEPM Special Publication 84, p. 397-520.

Powell, R. D. and Cooper, J. M., 2002, A glacial sequence stratigraphic model for temperate, glaciated continental shelves, in Dowdeswell, J.A. and O Cofaigh, C. eds., Glacier-influenced sedimentation on high-latitude continental margins: Geological Society of London, Special Publications 203, p. 215-244.

Powell, R.D., and Domack, E., 2002, Modern glaciomarine environments. Modern and past glacial environments. J. Menzies. Oxford, Butterworth-Heinemann Ltd., p. 361-389.

Ramos, V.A., 2008, Patagonia: A Paleozoic continent adrift: Journal of South American Earth Sciences, v. 26, p. 235-251.

Ramos, V.A., Naipauer, M., 2014, Patagonia: where does it come from?: Journal of

Iberian Geology 40, p. 367-379.

Rapalini, A.E., López de Luchi, M., Martínez Dopico, C., Lince Klinger, F., Giménez, M., Martínez, P., 2010. Did Patagonia collide with Gondwana in the Late Paleozoic? Some insights from a multidisciplinary study of magmatic units of the North Patagonian Massif: Geologica Acta 8, p. 349-371.

Rapela, C.W., Pankhurst, R.J., Harrison, S.M., 1989. Gondwana Plutonism of Northern Patagonia. 28th International Geological Congreso, Washington DC, Abstracts, vol. 2, p. 675.

Rygel, M. C., Fielding, C. R., Frank, T. D., and Birgenheier, L. P., 2008, The magnitude of late Paleozoic glacioeustatic fluctuations: a synthesis: Journal of Sedimentary Research, v. 78, p. 500-511.

Shanmugam, G., Lehtonen, L. R., Straume, T., Syvertsen, S.E., Hodgkinson, R. J., and Skibeli, M., 1994, Slump and debris-flow dominated upper slope facies in the Cretaceous of the Norwegian and northern North Seas (61-67 degrees N): implications for sand distribution: American Association of Petroleum Geologists Bulletin, v. 78, no. 6, p. 910-937.

Shanmugam, G., 2006, Deep-water processes and facies models: implications for sandstone petroleum reservoirs, Amsterdam, Elsevier, 475 p.

Smith, J.V., 2000, Flow pattern within a Permian submarine slump recorded by oblique folds and deformed fossils, Ulladulla, south-eastern Australia: Sedimentology, v. 47, p. 357-366.

Steel, R., and Olsen, T., 2002, Clinoforms, Clinoform Trajectories and Deepwater Sands, Sequence Stratigraphic Models for Exploration and Production: Evolving Methodology, Emerging Models, and Application Histories: 22nd Annual, Volume 22, Society of Economic Paleontologists and Mineralogists, p. 367-380.

Steel, R.J., Carvajal, C., Petter, A.L., and Uroza, C., 2008, Shelf and shelf-margin growth in scenarios of rising and falling sea level: Special Publication - Society for Sedimentary Geology, v. 90, p. 47-71.

Strachan, L. J., 2002, Slump-initiated and controlled syndepositional sandstone remobilization: an example from the Namurian of County Clare, Ireland: Sedimentology, v. 49, no. 1, p. 25-41.

Strachan, L. J., 2008, Flow transformations in slumps: a case study from the Waitemata Basin, New Zealand: Sedimentology, v. 55, p. 1311-1332.

Sumner, E.J., Talling, P.J., Amy, L.A., Wynn, R.B., Stevenson, C.J., and Frenz, M.,

2012, Facies architecture of individual basin-plain turbidites: Comparison with existing models and implications for flow processes: Sedimentology, v. 59, p. 1850-1887.

Taboada, A.C., 2008. First record of the Late Palaeozoic brachiopod Verchojania Abramov in Patagonia, Argentina: Proceedings of the Royal Society of Victoria, v. 120, no. 1, p. 305–319.

Taboada, A. C., 2010, Mississippian-Early Permian brachiopods from western Argentina: Tools for middle- to high-latitude correlation, paleobiogeographic and paleoclimatic reconstruction: Palaeogeography, Palaeoclimatology, Palaelecology, v. 298, p. 152-173.

Taboada, A.C. and Pagani, M.A., 2010, The coupled occurance of *Cimmeriella Jakutoproductus* (Brachiopoda: Productidina) in Patagonia: implications for Early Permian high to middle paleolatitudinal correlations and paleoclimatic reconstruction: Geologica Acta, v. 8, n. 4, p. 513-534.

Taboada, A.C. and Shi, G.R., 2011, Taxonomic review and evolutionary trends of Levipustulini and Absenticostini (Brachiopoda) from Argentina: palaeobiogeographic and palaeoclimatic implications. Memoirs of the Association of Australasian Palaeontologists 41, 87-114.

Talling, P. J., Amy, L. A., Wynn, R. B., Peakall, J. and Robinson, M., 2004, Beds comprising debrite sandwiched within co-genetic turbidite: origin and widespread occurrence in distal depositional environments: Sedimentology, v. 51, p. 163–194.

Talling, P. J., Amy, L. A., and Wynn, R. B., 2007, New insights into the evolution of large volume turbidity currents; comparison of turbidite shape and previous modelling results: Sedimentology, v. 54, p. 737-769.

Talling, P.J., Masson, D.G., Sumner, E.J., and Malgesini, G., 2012, Subaqueous sediment density flows: Depositional processes and deposit types: Sedimentology, v. 59, no. 7, p. 1937-2003.

Thomas, G.S.P., and Connell, R. J., 1985, Iceberg drop, dump, and grounding structures from Pleistocene glacio-lacustrine sediments, Scotland: Journal of Sedimentary Petrology, v. 55, no. 2, p. 243-249.

Vakarelov, B.K., Ainsworth, R.B., and MacEachern, J.A., 2012, Recognition of wave dominated, tide-influenced shoreline systems in the rock record: Variations from a microtidal shoreline model: Sedimentary Geology, v. 279, p. 23-41.

Van Der Merwe, W.C., Hodgson, D.M., and Flint, S.S., 2011, Origin and terminal

architecture of a submarine slide: a case study from the Permian Vischkuil Formation, Karoo Basin, South Africa: Sedimentology, v. 58, p. 2012-2038.

Visser, J. N. J., 1997, Deglaciation sequences in the Permo-Carboniferous Karoo and Kalahari basins of southern Africa: a tool in the analysis of cyclic glaciomarine basin fills: Sedimentology, v. 44, p. 507-521.

Wallace, K. and Eyles, N., 2015, Seismites within ordovician-silurian carbonates and clastics of southern ontario, canada and implications for intraplate seismicity: Sedimentary Geology, v. 316, p. 80-95.

Ziegler, A. M., Hulver, M.L., and Rowley, D.B., 1997, Permian World topography and climate, in Martini, I.P., ed., Late Glacial and Postglacial Environmental Changes: Quaternary Carboniferous-Permian, and Proterozoic: Oxford University Press, Oxford, U.K., p. 111-146.

Appendix:

Stratigraphic Columns

Pampa de Tepuel Formation


Clay
Silt
Sand
VF
F
M
C
VC
Gravel

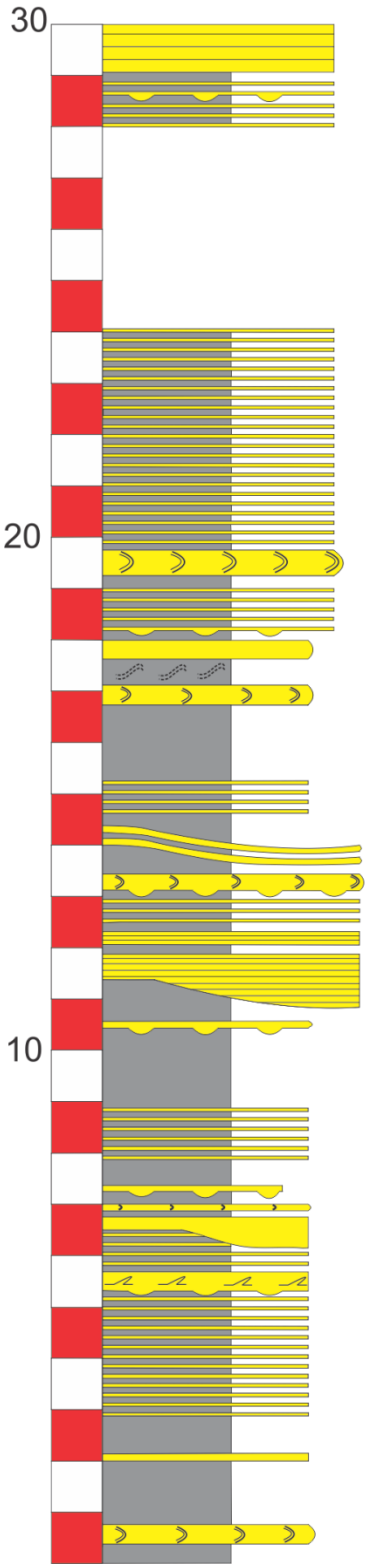
30
20
10

THN-1

0-30 m

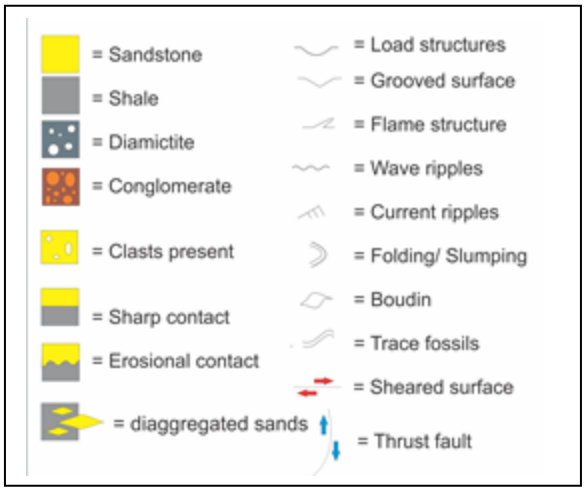
= Sandstone
= Shale
= Diamictite
= Conglomerate
= Clasts present
= Sharp contact
= Erosional contact
= diaggregated sands
= Load structures
= Grooved surface
= Flame structure
= Wave ripples
= Current ripples
= Folding/ Slumping
= Boudin
= Trace fossils
= Sheared surface
= Thrust fault

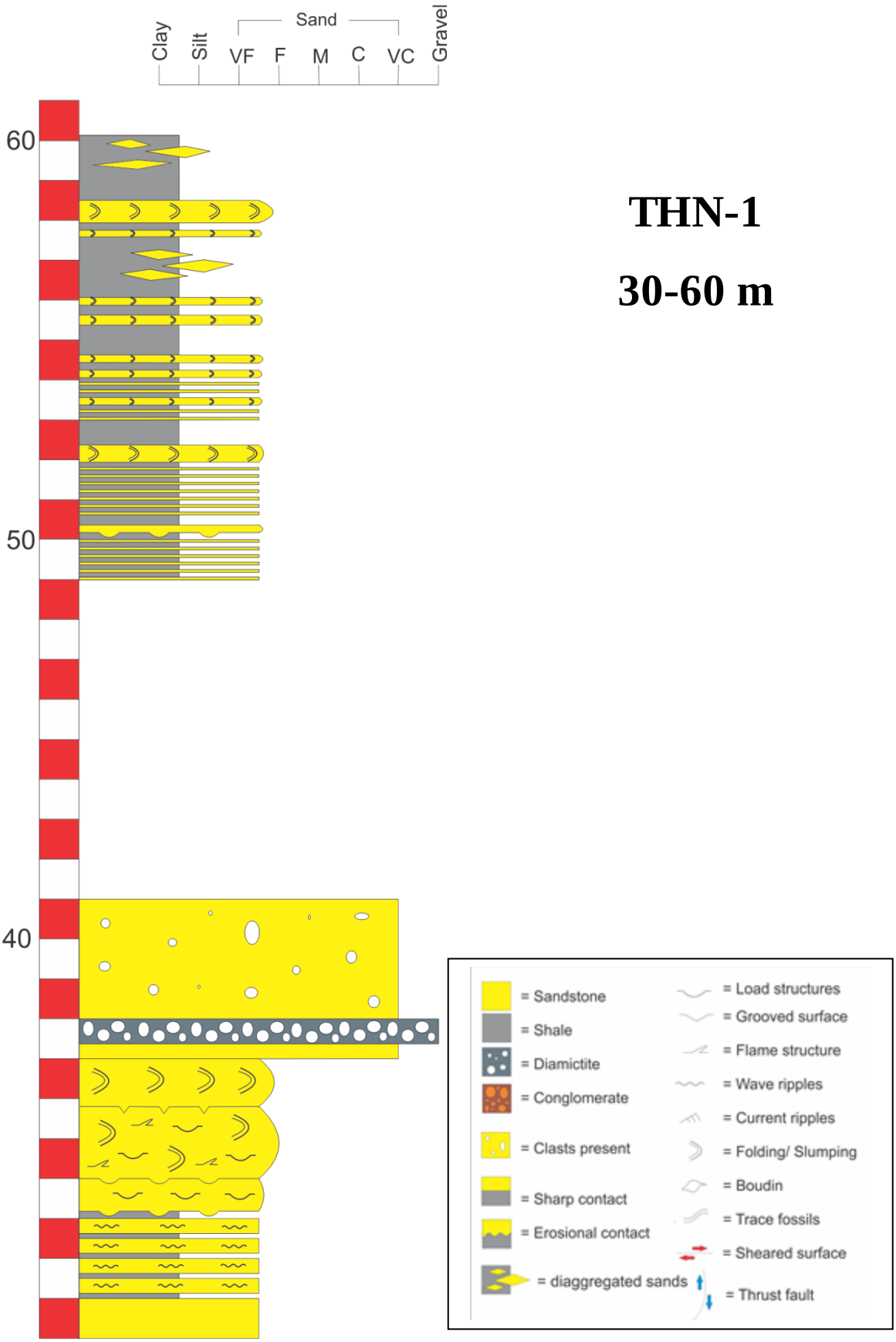
Clay
Silt
Sand
VF
F
M
C
VC
Gravel
60
50
40
= Sandstone
= Shale
= Diamictite
= Conglomerate
= Clasts present
= Sharp contact
= Erosional contact
= diaggregated sands
= Load structures
= Grooved surface
= Flame structure
= Wave ripples
= Current ripples
= Folding/ Slumping
= Boudin
= Trace fossils
= Sheared surface
= Thrust fault

THN-1

30-60 m

THN-1

61-70 m

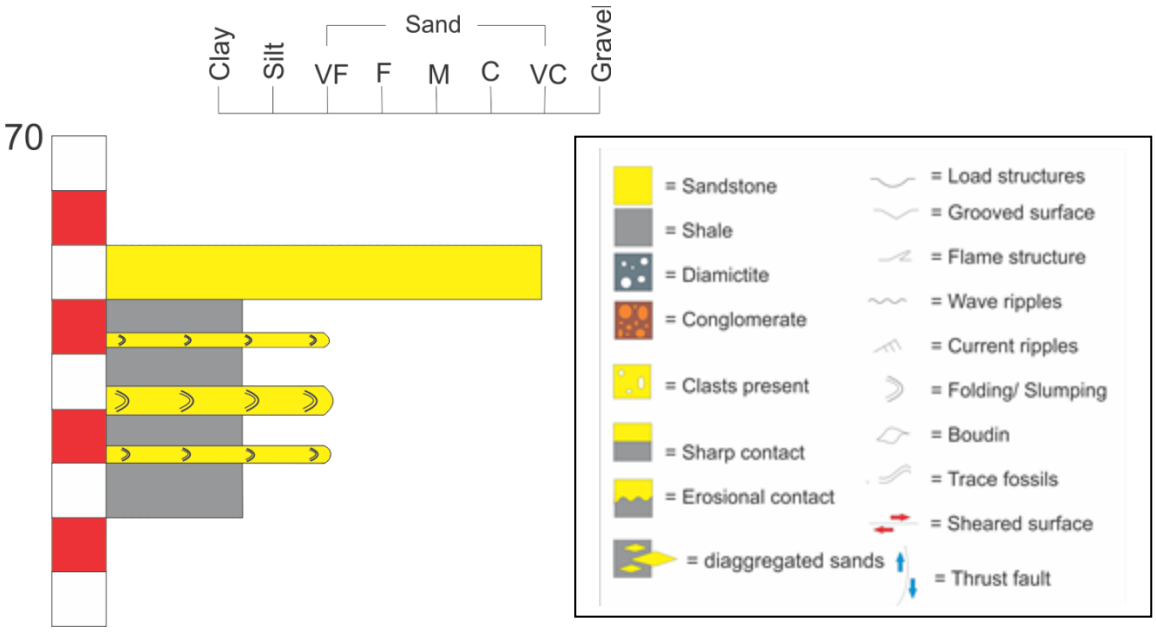
Clay
Silt
Sand
VF
F
M
C
VC
Gravel
70
= Sandstone
= Shale
= Diamictite
= Conglomerate
= Clasts present
= Sharp contact
= Erosional contact
= diaggregated sands
= Load structures
= Grooved surface
= Flame structure
= Wave ripples
= Current ripples
= Folding/ Slumping
= Boudin
= Trace fossils
= Sheared surface
= Thrust fault

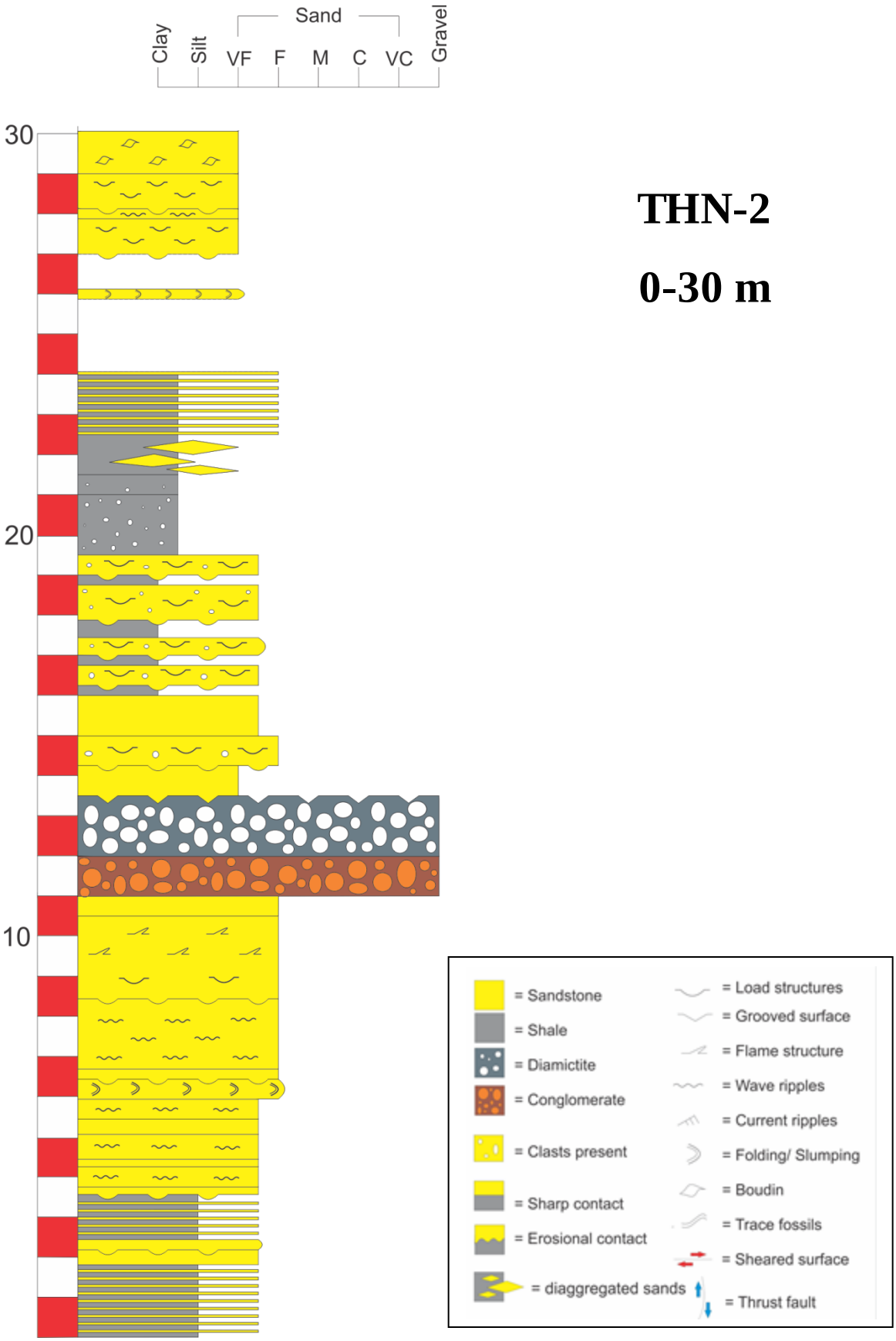
Clay
Silt
Sand
VF
F
M
C
VC
Gravel
30
20
10
THN-2
0-30 m
= Sandstone
= Shale
= Diamictite
= Conglomerate
= Clasts present
= Sharp contact
= Erosional contact
= diaggregated sands
= Load structures
= Grooved surface
= Flame structure
= Wave ripples
= Current ripples
= Folding/ Slumping
= Boudin
= Trace fossils
= Sheared surface
= Thrust fault

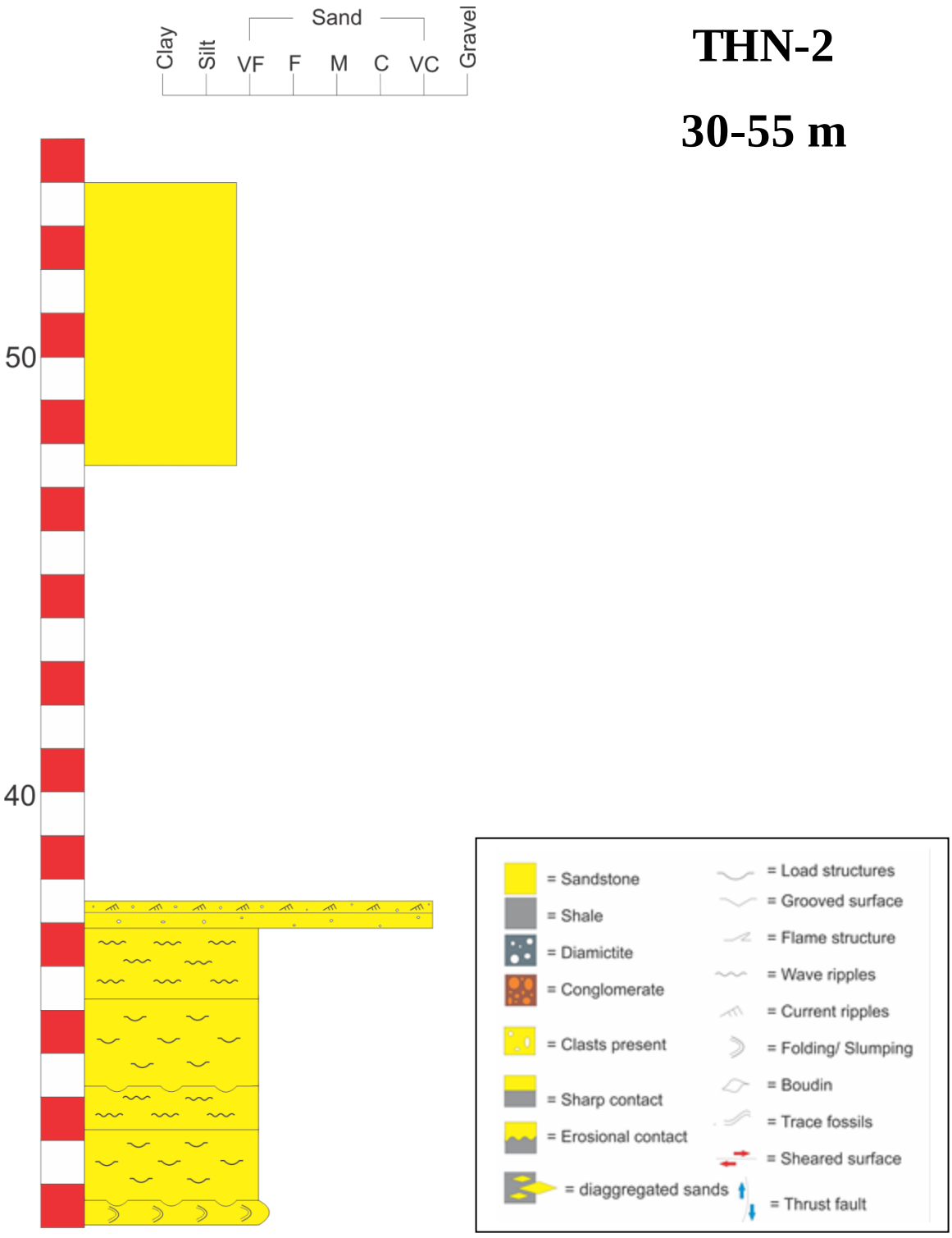
Clay
Silt
Sand
VF
F
M
C
VC
Gravel
50
40
= Sandstone
= Shale
= Diamictite
= Conglomerate
= Clasts present
= Sharp contact
= Erosional contact
= diaggregated sands
= Load structures
= Grooved surface
= Flame structure
= Wave ripples
= Current ripples
= Folding/ Slumping
= Boudin
= Trace fossils
= Sheared surface
= Thrust fault

THN-2

30-55 m

THN-3

Complete section

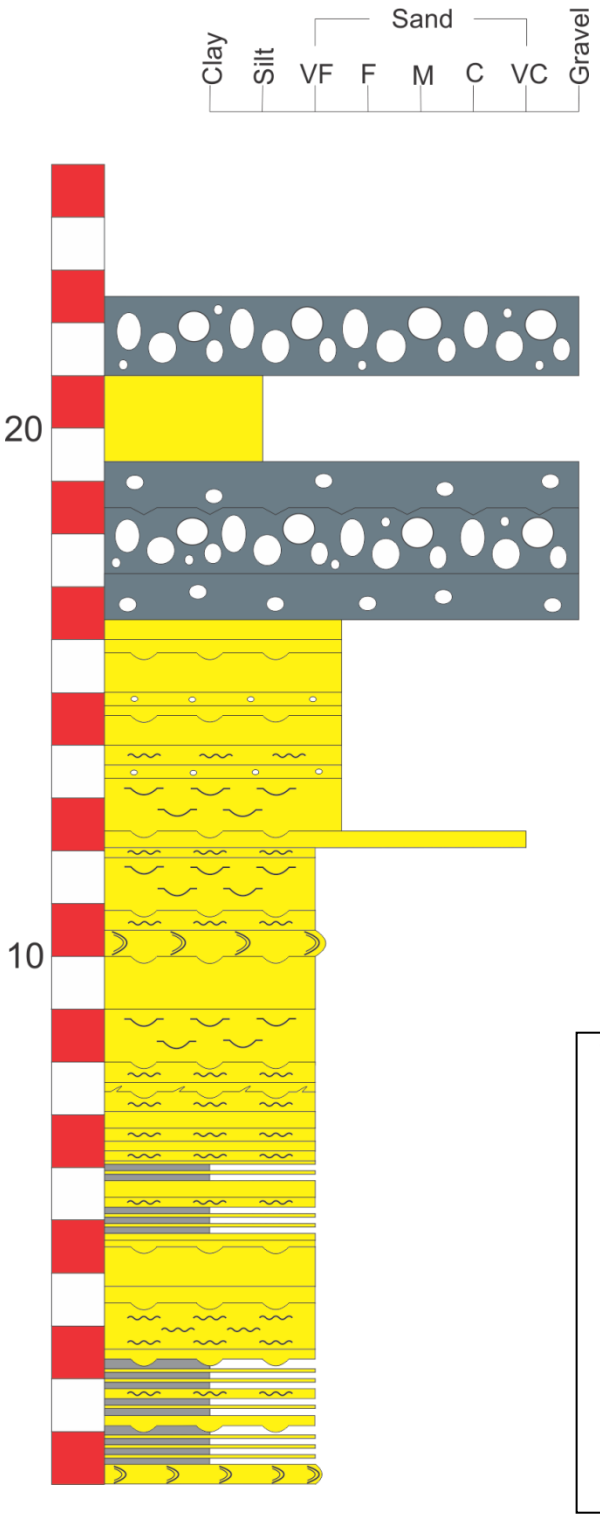

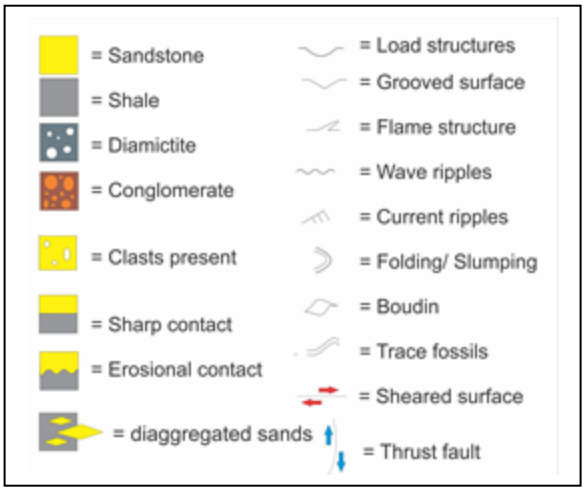

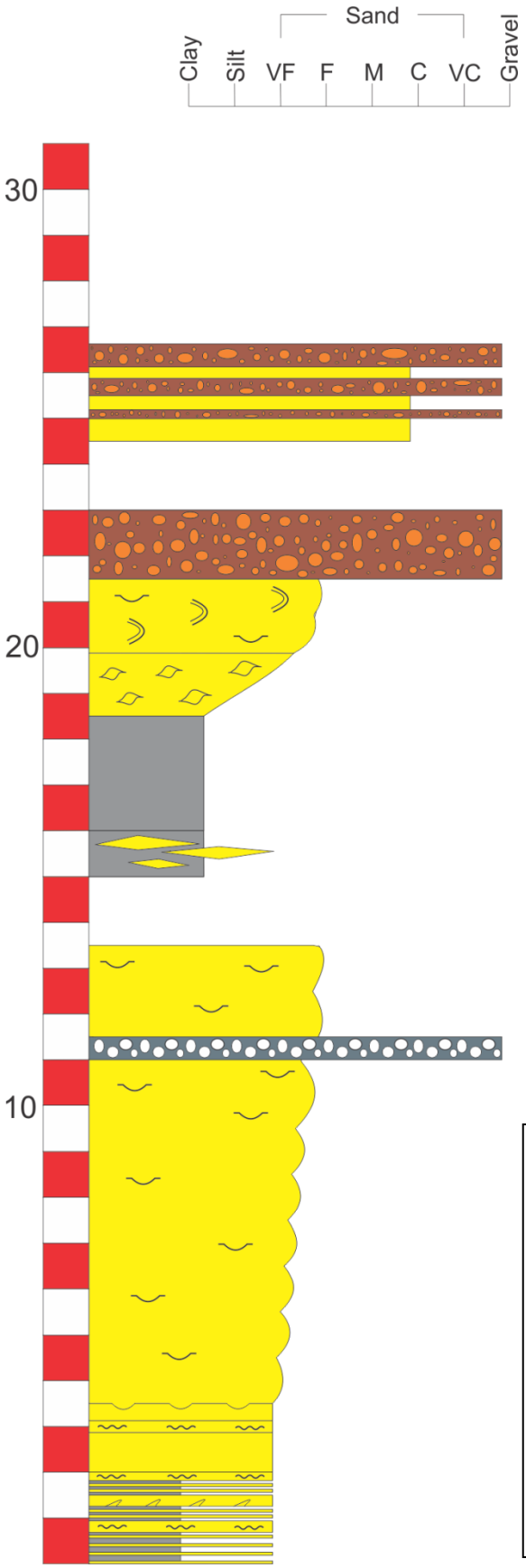

THN-4

0-30 m

= Sandstone
= Shale
= Diamictite
= Conglomerate
= Clasts present
= Sharp contact
= Erosional contact
= diaggregated sands
= Load structures
= Grooved surface
= Flame structure
= Wave ripples
= Current ripples
= Folding/ Slumping
= Boudin
= Trace fossils
= Sheared surface
= Thrust fault

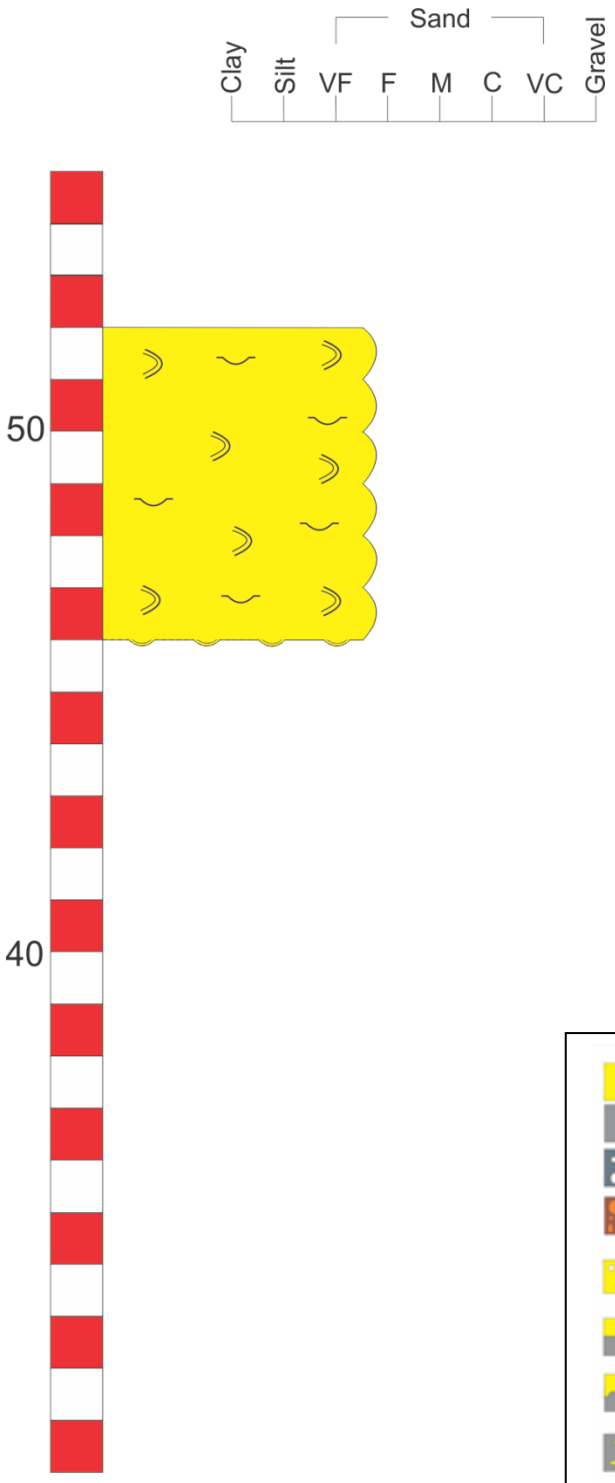
Sand
Clay
Silt
VF
F
M
C
VC
Gravel
50
40

THN-4

30-55 m

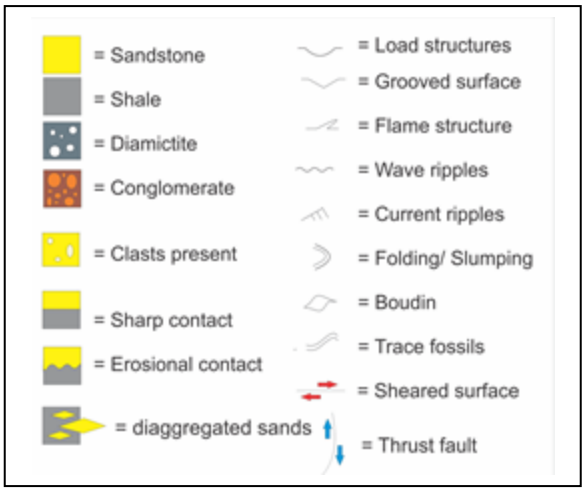
= Sandstone
= Shale
= Diamictite
= Conglomerate
= Clasts present
= Sharp contact
= Erosional contact
= diaggregated sands
= Load structures
= Grooved surface
= Flame structure
= Wave ripples
= Current ripples
= Folding/ Slumping
= Boudin
= Trace fossils
= Sheared surface
= Thrust fault

THN-5

Complete section

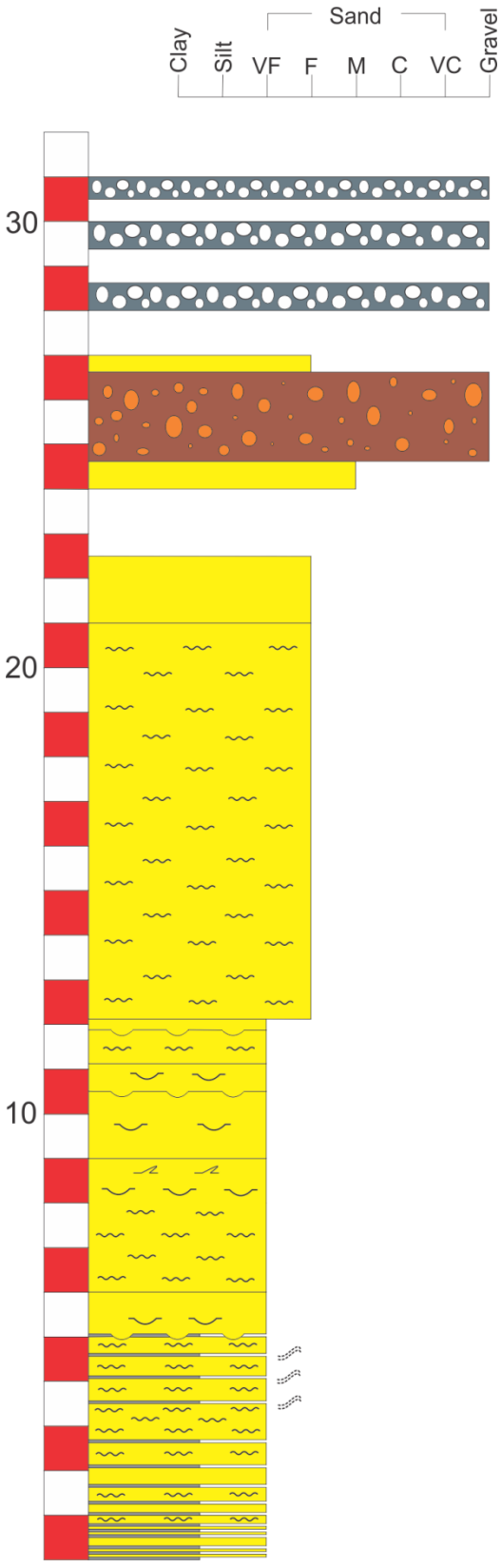

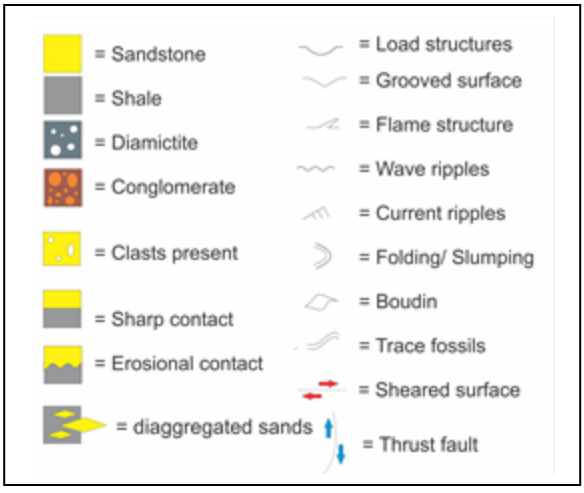

THN-6

Complete section